Annu. Rev. Phys. Chem. 2001. 52:279–313

PULSED EPR SPECTROSCOPY: Biological Applications

Thomas Prisner, Martin Rohrer, and Fraser MacMillan
Institute for Physical and Theoretical Chemistry, J. W. Goethe-University Frankfurt, Marie-Curie-Strasse 11, D-60439 Frankfurt am Main, Germany;
e-mail: prisner@chemie.uni-frankfurt.de

Dedicated to the memory of Jerry Babcock

Key Words pulsed ENDOR, ESEEM, high-field EPR, enzymes, paramagnetic centers

■ **Abstract** Pulsed electron paramagnetic resonance (EPR) methods such as ESEEM, PELDOR, relaxation time measurements, transient EPR, high-field/high-frequency EPR, and pulsed ENDOR, have been used successfully to investigate the local structure and dynamics of paramagnetic centers in biological samples. These methods allow different contributions to the EPR spectra to be distinguished and can help unravel complicated EPR spectra consisting of overlapping resonance lines, as are often found in disordered protein samples. The basic principles, specific potentials, technical requirements, and limitations of these advanced EPR techniques will be reviewed together with recent applications to metal centers, organic radicals, and spin labels in proteins.

INTRODUCTION

Electron paramagnetic resonance (EPR) spectroscopy is a well-known method for the examination of the local structure of paramagnetic molecules. In proteins such paramagnetic molecules can be naturally stable cofactors (e.g. heme molecules, iron-sulfur clusters, or metal ions); transiently generated radicals within a reaction cycle (chromophores, cofactors, or amino acid radicals); or artificial nitroxide spin labels attached to the protein. In contrast to nuclear magnetic resonance (NMR), EPR is not restricted by the size of the protein because only the paramagnetic centers and their interaction with the protein are spectroscopically visible. In cases in which only one paramagnetic center is located within the protein a simple one-dimensional (1D) continuous wave (cw) EPR experiment can give detailed information about the properties of the paramagnetic species, such as its oxidation state, ligand symmetry, and concentration. In more realistic cases, as in enzymes, the situation is far more complex: Often more than one paramagnetic species is involved (some of them may be transiently formed within the catalytic cycle of

the enzyme), which are also subjected to internal dynamics. In these cases the simple cw-EPR spectra will suffer from the same difficulties as NMR for large molecules: Spectral lines overlap and broaden. Therefore, it becomes very difficult to analyze the spectra quantitatively and to obtain a unique solution; the problem is ill defined. As in NMR, pulse methods help unravel the different contributions to 1D-EPR spectra. Overlapping spectral components of different paramagnetic centers may be separated by pulsed EPR methods, for example by their relaxation times or by their spin-magnetic moment.

Whereas the methodological principles for the manipulation of the spin system (electron spin S in EPR, nuclear spin I in NMR) are very similar in NMR and EPR spectroscopy, the technical requirements and therefore the practical realization is quite different in both fields. Owing to the much larger magnetic moment of the electron spin S (nearly a factor of 1000 larger compared with a proton nuclear spin) the technical requirements (resonance frequency, relaxation times, pulse lengths) for EPR are much more demanding as compared with NMR spectroscopy. Nevertheless, most of the technical restrictions have been overcome by the development of specific pulse methods and techniques. These methods can, similar to heteronuclear NMR spectroscopy, not only affect the unpaired electron of a single paramagnetic species, but at the same time affect magnetically coupled nuclear spins as in pulsed electron nuclear double resonance (ENDOR) or the electron spin of another paramagnetic center in pulsed electron double resonance (PELDOR) experiments. Whereas in the experiments mentioned above the nuclear spin or the additional electron spin are excited by a second radiofrequency (RF) or microwave (MW) pulse, in many cases both types of couplings can also be examined with a single MW pulse in resonance with the unpaired electron spin. These methods are called electron spin echo envelope modulation (ESEEM) for the investigation of nuclear couplings and "2 + 1" for the examination of coupling to other paramagnetic centers. A further dimension can be added if they are performed at different external magnetic fields. Experiments at high magnetic fields (>2 T), especially, have proven to significantly enhance the amount of information that can be gathered from EPR and ENDOR spectra of aromatic organic radicals in proteins. All these advanced EPR techniques have dramatically increased the potential of EPR spectroscopy, especially in the field of biochemical applications. Nevertheless, it should be mentioned that for all biological systems discussed in this review, cw-EPR and cw-ENDOR methods have preceded the pulsed EPR investigations and have built a most valuable starting base for the advanced investigations reviewed herein.

PULSED METHODS AND RECENT APPLICATIONS TO BIOLOGICAL SYSTEMS

Technical Aspects

Unfortunately, one of the main advantages of pulsed NMR spectroscopy—the enhanced sensitivity of pulsed Fourier transform (FT) spectroscopy—does not apply

to EPR spectroscopy on biological samples. In contrast to NMR spectroscopy, the rotational correlation time of biological macromolecules at room temperature is in most cases much too slow to effectively average the large anisotropic interactions of the unpaired electron spin. This leads to broad unresolved lineshapes—in many cases much broader than the available pulse excitation width, so that only a part of a spectrum can be recorded at a given magnetic field value. Therefore, the multiplex advantage of the pulsed experiments—recording of several lines at the same time—does not apply to EPR on macromolecules. Additionally, because of these broad linewidths and the very short relaxation times of paramagnetic centers, e.g. for transition metal ions, the pulse lengths have to be very short. To allow the short MW pulses to pass through the cavity circuit the bandwidth of the resonant MW cavity usually has to be lowered, as compared with cw-applications. This reduction of the Q value of the pulsed resonant circuits leads to a lower sensitivity.

Consequently, the only reason to perform pulsed experiments on proteins is the possibility of enhancing the spectral information on spin systems, as mentioned above. In many cases the lineshape of the paramagnetic center is inhomogeneously broadened in protein samples, owing to orientationally disordered samples or other inhomogeneities in the protein. Thus, most of the interesting interactions of the paramagnetic center with its surrounding, as for example the hyperfine coupling (hfc) to magnetic nuclei in the close surrounding, are hidden under these broadening mechanisms and cannot be observed directly in cw-EPR experiments. Pulsed experiments can refocus such static inhomogeneous broadening contributions and dramatically increase the spectral resolution with respect to other interactions, such as hfcs to nuclei or dipolar couplings to other paramagnetic species. Despite the fact that the MW pulses in pulsed EPR are by far less ideal than in NMR spectroscopy, the possibility of manipulating the spin system is still of great advantage in unraveling the information content of spectra in complex spin systems, by suppressing specific interactions and by diluting the spectra in a more-dimensional spectral space.

As already mentioned, the requirements on the equipment for pulsed EPR measurements are demanding. Pulse lengths have to be well below 100 ns, typically 5–10 ns for a $\pi/2$-pulse at X-band MW frequencies with a 1 kW MW amplifier. Care has to be taken that the bandwidth of all components in the excitation and detection channel support these short pulses without distortion. The important limitation for the observation of species with short transverse relaxation times is the dead time of the receiver after intense MW pulses. Typically, this time is about 50 ns and limits the detection to systems with longer transverse relaxation times T_2. It also makes it difficult to observe the free induction decay signal of most samples. For many paramagnetic ions the longitudinal relaxation time T_1 is also short even at low temperature. Only very recently have fast signal digitizers ($>10^8$ points/s, 8 bit resolution) and averagers ($>10{,}000$ acquisition/s, 1024 data points) been available for effective data collection with an optimum duty cycle (1). Fortunately, pulsed experiments put less stringent requirements on MW source noise, cavity stability, microphonics, and other sources of noise and baseline drift. This allows the less sensitive and therefore more time consuming pulsed

experiments to be performed even on biological systems with low spin concentrations.

Spin Hamilton Operator

The magnetic properties of the unpaired electron spin of a paramagnetic center can be described by a spin Hamilton operator of the form (2):

$$H = \beta_e \vec{S}_p \cdot \hat{g} \cdot \vec{B}_0 + \sum_j \gamma_j \cdot \vec{I}_j \cdot \vec{B}_0 + \sum_j \vec{S}_p \cdot \hat{A}_j \cdot \vec{I}_j + \sum_j \vec{I}_j \cdot \hat{Q}_j \cdot \vec{I}_j + \sum_k \vec{S}_p \cdot \hat{D}_{pk} \cdot \vec{S}_k + \vec{S}_p \cdot \hat{D}_{pp} \cdot \vec{S}_p \qquad 1.$$

The first term represents the interaction of the unpaired electron spin $\vec{S}_p$ with the external magnetic field $\vec{B}_0$ via the anisotropic g-tensor of the paramagnetic molecule. The next two terms represent the magnetic interactions of close-by nuclear spins $\vec{I}_j$ with the external magnetic field and with the electron spin via the hfc tensor $\hat{A}$. The fourth term is the quadrupolar interaction $\hat{Q}$ for nuclear spins with $I > 1/2$. The remaining terms are the interaction of the paramagnetic center with other unpaired electron spins $\vec{S}_k$, including dipolar and exchange contributions and the so-called zero field splitting for electron spins $S > 1/2$. This Hamilton operator can be simplified for specific types of centers under many conditions, where one or two terms in the Hamilton operator dominate the spectra. Although ENDOR or ESEEM experiments are only sensitive to the interaction to other close-by nuclei within a distance range of up to 0.8 nm, PELDOR and pulsed EPR relaxation experiments are sensitive to dipolar interaction to other paramagnetic centers with distances up to approximately 5 nm. High magnetic field experiments can resolve the anisotropy of the electronic g-tensor, whereas this anisotropy is suppressed for most aromatic organic radicals at lower magnetic fields. Therefore, these different experiments can help distinguish between these contributions to the spin Hamilton operator and allow, even for complex systems, a detailed understanding of the paramagnetic center.

For a theoretical description of pulsed experiments, the time evolution of the quantum mechanical system under nonstationary perturbations (by MW and/or RF excitation) has to be considered. These can be described with the density matrix of the spin system including the excitation fields and spin interactions. The time evolution of the spin system is given by the stochastic Liouville equation, which has to be solved. Nevertheless, the basics of most of the pulsed experiments can be understood on the basis of simple energy level diagrams, in which only the eigenfunctions and eigenvalues of the spin Hamilton operator without excitation perturbation are considered.

In Figure 1 the resulting energy level scheme and spin eigenfunctions are shown for two simple cases: (*a*) the coupling of an unpaired electron spin $S = 1/2$ to a single nuclear spin $I = 1/2$ and (*b*) the coupling of two unpaired electron spins $S_1 = 1/2$ and $S_2 = 1/2$. The spin Hamiltonian eigenfunctions, when expressed in the

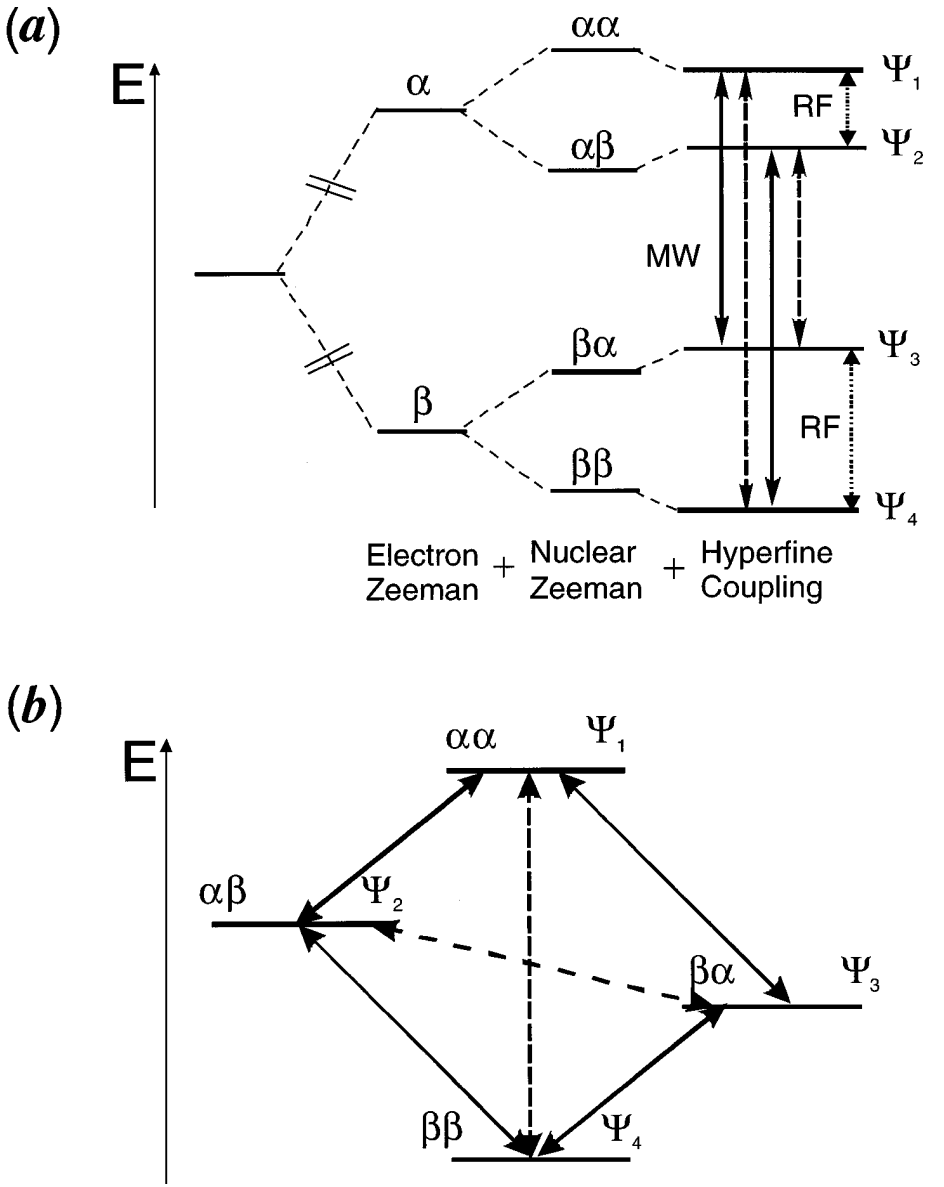

Figure 1 Energy level diagram for (*a*) an electron spin $S = 1/2$ coupled to a nuclear spin $I = 1/2$ and (*b*) two electron spins $S_1 = 1/2$ and $S_2 = 1/2$. The high-field basis functions α (m_S or $m_I = +1/2$) and β (m_S or $m_I = -1/2$) for the eigenfunctions $\Psi_1 - \Psi_4$ are valid only without coupling of the two spins. Allowed (solid arrows) and 'forbidden' EPR (dashed arrows) and NMR (dotted arrows) transitions between the spin states are included.

high-field eigenfunctions, α and β, are mixed states owing to anisotropic tensor interactions [hfc tensor $\hat{A}$ in (*a*) and dipolar and exchange coupling tensor $\hat{D}$ in (*b*)]. As a consequence of this mixing of the eigenfunctions, all transitions between the four eigenstates are allowed to a different extent under pulsed irradiation of the spin system. However, in case (*a*) the energy spacing by the nuclear and the electronic magnetic moment differs by approximately three orders of magnitude (much larger than shown in the diagram); hence, MW pulses only affect EPR transitions and RF pulses only affect NMR transitions of the coupled spin system. Because of the large hfc, RF pulses select a single NMR transition in only one electron spin manifold (α or β) in most cases, e.g. will induce transitions either between $\Psi_1 \leftrightarrow \Psi_2$ or $\Psi_3 \leftrightarrow \Psi_4$. In contrast, MW pulses select a single EPR transition (e.g. only $\Psi_1 \leftrightarrow \Psi_3$) or semiselective ($\Psi_1 \leftrightarrow \Psi_3$ and $\Psi_2 \leftrightarrow \Psi_4$). Two further EPR transitions will be partially allowed because of the mixing of the nuclear spin states by the anisotropic hfc (between state $\Psi_1 \leftrightarrow \Psi_4$ and $\Psi_2 \leftrightarrow \Psi_3$), as shown by the dashed lines in Figure 1.

Pulsed Electron Nuclear Double Resonance (Pulsed ENDOR)

Cw-ENDOR was first introduced by Feher (3). It was rapidly demonstrated to be a powerful tool to significantly increase spectral resolution as compared with cw-EPR. Analogous pulsed methods have been introduced by Mims (4) and Davies (5). Today cw and pulsed ENDOR techniques are well-established advanced EPR methods, being commonly applied in biology and organic chemistry.

Regardless of whether they are performed in a cw or pulsed mode, all ENDOR experiments have an EPR signal that is monitored, during which NMR transitions are induced that lead to changes of the EPR signal. These changes of an EPR signal are recorded as the ENDOR spectrum.

A thorough theoretical description of ENDOR methods is complex and requires significant mathematical and physical background knowledge (for review see 6, 7). Nevertheless, a simple energy level consideration (see Figure 1) allows a phenomenological understanding that is sufficient to explain the advantages and limitations of the method. In particular, the pulsed Davies ENDOR experiment can be explained in this picture quite easily. The description is based on a system characterized solely by an electron spin $S = 1/2$ and a nuclear spin $I = 1/2$. Owing to the applied static magnetic field B_0, the energy levels of the two quantum spin states α and β, both for S and I, are no longer degenerate. The resulting electron and nuclear Zeeman energy splittings differ by roughly three orders of magnitude as the result of the different electronic and nuclear gyromagnetic ratios. Furthermore, the hfc between the electronic and nuclear spins leads to an increase/decrease of the nuclear Zeeman splitting between the α and β electronic spin states. According to quantum mechanical selection rules, EPR transitions with $\Delta m_S = 1$ and $\Delta m_I = 0$ and NMR transitions with $\Delta m_I = 1$ and $\Delta mS = 0$ are allowed. During the basic pulsed Davies ENDOR experiment one of the EPR transitions is selectively induced (by a MW π-pulse) and monitored (by a MW Hahn echo

pulse sequence) as shown in Figure 2. Under ideal conditions, the echo signal is thereby inverted as a result of the inversion pulse at the beginning of the sequence. This holds if the longitudinal relaxation time T_1^S is much longer than the pulse separation time T (see Figure 2). Selective excitation of one of the NMR transitions by the additional RF pulse will now change the detected EPR echo signal, which is the ENDOR effect. The echo can disappear completely if the RF matches exactly one of the two allowed NMR transition frequencies and if

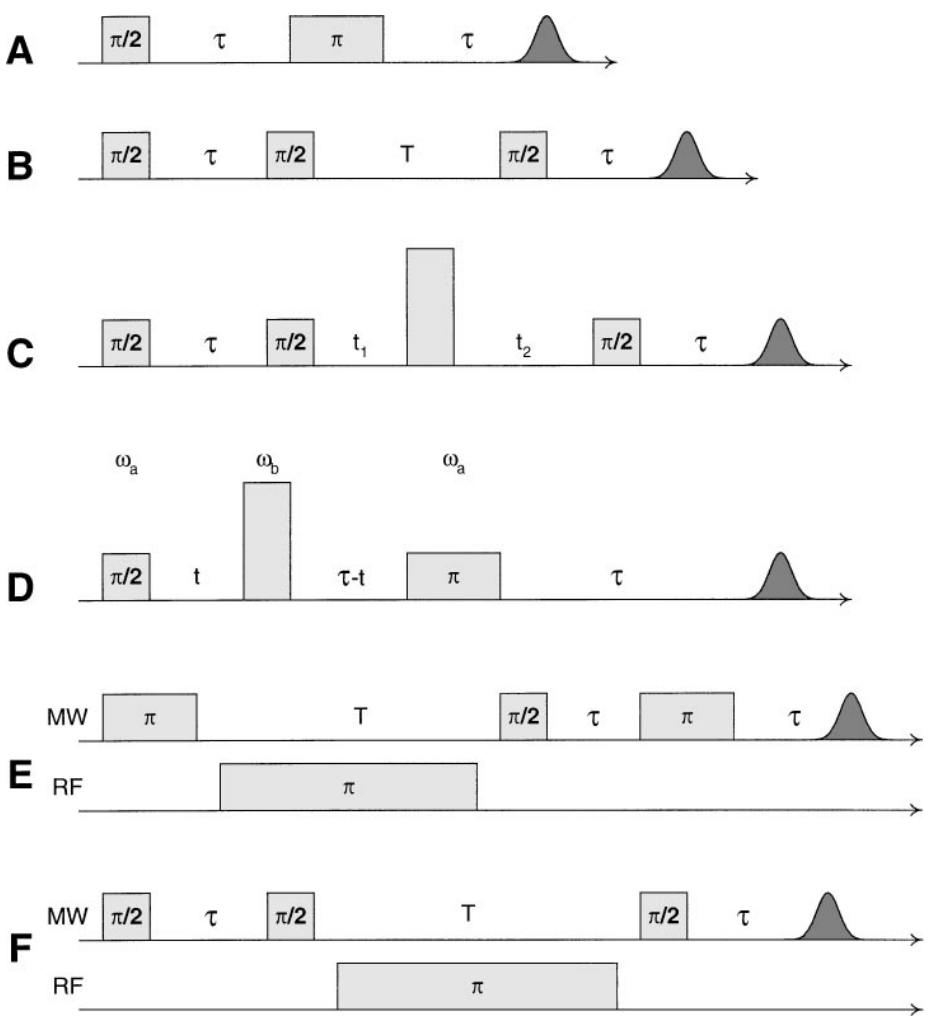

Figure 2 Pulsed-EPR and ENDOR experiments described in text. (*A*) Two-pulse (Hahn) echo, (*B*) three-pulse (stimulated) echo, (*C*) four-pulse echo (HYSCORE), (*D*) PELDOR pulse (for $\omega_a = \omega_b$, which corresponds to the "2 + 1" pulse sequence), (*E*) Davies ENDOR, (*F*) Mims ENDOR.

the pulse flip angle corresponds to a RF π-pulse for the nuclear spin. During the experiment the RF is swept linearly in time and the ENDOR spectra are recorded as a function of the RF. As can be rationalized from Figure 1, the magnitude of the observed hyperfine splitting is directly reflected in the frequency spacing between the two ENDOR signals. This applies for cases in which the hfc is small compared with the nuclear Zeeman energy at the chosen magnetic field if no further interactions such as zero field splitting or quadrupolar interactions have to be considered.

The technical effort required to generate strong RF fields over a broad frequency range to the cavity is rather high and quite expensive. Fortunately, over the past two decades, the instrumentation for extending EPR experiments to ENDOR capability has become readily available.

The basic advantages of ENDOR are the drastic increase of hyperfine resolution. Additionally, when a large number of equivalent nuclei interact with the electronic spin, the ENDOR spectra are significantly simplified compared with the corresponding EPR spectra. Drawbacks of ENDOR, especially when powder-type ENDOR spectra are to be interpreted, arise from overlapping lines originating from different interacting nuclei. These can be overcome by high-field ENDOR (see "Pulsed High-Field/High-Frequency EPR") or by application of advanced ENDOR methods (8, 9).

Another difficulty in the interpretation is often encountered if the observed hfc is larger than twice the nuclear Zeeman interaction. The ENDOR frequencies ν_{ENDOR} are given (for the simple cases under consideration) by:

$$\nu_{ENDOR} = \left|\nu_n \pm \frac{A}{2}\right|, \quad \nu_n = \frac{g_n \mu_n B_0}{h} \qquad 2.$$

where g_n and μ_n are the nuclear g-factor and the nuclear magneton, respectively, h is the Planck's constant, and A is the hfc. In cases in which the free nuclear ENDOR frequency ν_n is greater than $|A/2|$, the ENDOR lines are centered symmetrically around ν_n. In contrast, if ν_n is smaller than $|A/2|$ the ENDOR lines are centered around $|A/2|$ with a spacing corresponding to $2\nu_n$. This complicates the distinct assignment of ENDOR lines and makes the interpretation more difficult. One obvious way around this problem is the performance of ENDOR at different magnetic fields and frequencies because ν_n depends on the magnetic field B_0, whereas hfc does not.

Further important parameters to be considered concern the spin relaxation times of the system under investigation: For cw experiments, the most pronounced ENDOR effect is normally obtained when the longitudinal electronic (T_1^S) and nuclear spin relaxation (T_1^I) constants are equal, leading to the largest changes of the saturated EPR transition under observation. This condition can often be adjusted by means of sample temperature and solvent viscosity. It can also be overcome by advanced methods such as electron-nuclear-nuclear resonance (TRIPLE resonance), which has been applied successfully to measurements of organic radicals in liquid solution under physiological conditions (10). In contrast to cw-ENDOR, in

pulsed-ENDOR experiments the ratio T_1^S/T_1^I is not of importance for the ENDOR effect. Instead, the dominant requirement is that T_1^S must be long enough to allow for the application of an RF π-pulse within the pulse separation time T. Another limitation results from the transversal electronic spin relaxation time T_2^S, which has to be longer than the pulse separation time τ if an echo detection of the ENDOR effect is used (see Figure 2). Direct detection of the free induction decay may overcome this problem. Another limitation of ENDOR applications is found for very small hfcs: It is caused by the strength of the RF fields incident to the sample, which must not exceed the magnitude of the hfc under observation. If this happens NMR pulses are no longer selective, which reduces the ENDOR effect. Reducing the RF power, which however, also reduces the ENDOR effect if the pulse length cannot be prolonged at the same time, may eliminate this handicap. Further limitations of the ENDOR method arise for very small nuclear-level splittings (as is often the case for ^{2}H or ^{14}N at X-band frequencies) because of RF excitation problems at very low frequencies. A way around this problem is to apply ESEEM techniques, as described below.

Applications of ENDOR spectroscopy to biological systems have concentrated on organic radicals and metal ion centers in proteins. Both types of radicals are usually investigated at low temperature. Especially for metal centers the temperature has to be below 20 K in most cases to obtain long enough relaxation times allowing a successful ENDOR experiment.

Within the group of organic radicals the chromophores involved in the electron transfer reaction of photosynthetic proteins in particular have been extensively studied, not only by cw- but also by pulsed-ENDOR methods (for review see 11). The proton couplings of the two semiquinone electron acceptor radicals $Q_A^{-\bullet}$ and $Q_B^{-\bullet}$ in bacterial reaction centers (bRC) (12), of the first quinone acceptor $A_1^{-\bullet}$ in photosystem I (PSI) (13) and of the quinone $Q_A^{-\bullet}$ in photosystem II (PSII) have been investigated by pulsed ENDOR spectroscopy. Pulsed W-band (95 GHz, 3.4 T) ENDOR experiments on $Q_A^{-\bullet}$ of bRC (14) allowed full proton hfc tensorial information to be obtained, owing to the possibility of performing orientation-selective experiments at high fields, as explained below. In PSII proteins the two tyrosine radicals, redox active tyrosine 160 of the D2 protein of PSII ($Y_D^{-\bullet}$) and redox active tyrosine 161 of the D1 protein of PSII ($Y_Z^{-\bullet}$) have been actively investigated by a number of groups (15–18). Transient ENDOR (19) and pulsed ENDOR (20) have been used to investigate the triplet state of the primary chlorophyll donor $P_{865}^{+\bullet}$ of bRC. Pulsed-ENDOR spectroscopy was also applied to the transient correlated-radical pair $P_{700}^{+\bullet}A_1^{-\bullet}$ in PSI (21). Very recently both chlorophyll and carotene cation radicals in PSII were characterized by pulsed ENDOR (22).

Similar characterizations have been undertaken concerning protein-bound organic molecules. Pulsed ENDOR was used to examine the semiquinone of quinol oxidase (23), a methylamine dehydrogenase complex (24), a flavin radical in monoamine oxidase (25, 26), a spin-coupled tryptophan radical in cytochrome *c* peroxidase (27, 28), and the tyrosine radical of ribonucleotide reductase (29). On

the latter radical orientation-selective D-band (140 GHz, 5 T) ENDOR was also successfully applied to obtain tensorial information of the hfc tensors (30). The capability of the ENDOR method to distinguish different protein environments can be seen in Figure 3, in which pulsed-ENDOR spectra of such tyrosine radicals from different organisms are compared.

Applications of pulsed ENDOR to metalloenzymes, especially for Cu-proteins, FeS-centers, and binuclear Cu complexes, have been reviewed (31–35). ENDOR has been successfully used to determine ^{14}N-hfcs of the Cu ligands and ^{1}H/^{2}H couplings to ambient water molecules in the vicinity of the metal site (36, 37). Higher fields were used to gain more spectral information with Q-band ENDOR on azurin (38) and with W-band ENDOR on the Cu_A site of cytochrome *c* oxidase (39). The interaction of a Mn^{2+}-ion center with ATP has been investigated by pulsed ENDOR in pyruvate kinase (40) and compared with the ^{1}H-, ^{31}P-, and ^{17}O-hfc determined in model systems (41). The manganese cluster in PSII was also investigated by pulsed-ENDOR methods in its different catalytic states (42). High-field W-band ENDOR was recently used to study the manganese center in a single crystal of concavalin A (43). Also, the local surroundings of binuclear iron centers in uteroferrin and methane monooxygenases (44–47), the iron-molybdenum center of molybdoferredoxin (35, 48), the iron-sulfur centers of a number of iron-sulfur proteins (34, 49–52), and the heme centers of cytochrome P450 cam and chloroperoxidase (53–55) have been investigated by pulsed ENDOR.

Electron Spin Echo Envelope Modulation

The electron spin echo envelope modulation (ESEEM) effect is induced by nuclei hyperfine-coupled to the unpaired electron spin. These couplings manifest themselves in a periodic modulation of the electron spin echo intensity as a function of the pulse separation time. Fourier transformation of the time-domain echo envelope leads to a hyperfine spectrum in the frequency domain similar to the corresponding ENDOR spectrum. These modulations of the electron spin echo intensity due to the coupled nuclei were already observed in early electron spin echo experiments (56, 57) and later theoretically understood and analytically described (58–60).

For nuclei coupled to the electron spin via an anisotropic hyperfine interaction, 1D- and 2D-pulsed ESEEM experiments have proven to be powerful tools to examine these interactions, especially for weak couplings and for nuclei with a small Zeeman splitting (61). In contrast to the ENDOR experiment, no RF irradiation is needed; the nuclear spins are only indirectly affected via their hfc to the electron spin.

Figure 3 Pulsed Davies X-band ENDOR on tyrosyl radicals from three different organisms (F MacMillan, F Lendzian, A Boussac, G Lassmann, W Lubitz 2000, unpublished). (*A*) Y_D^{ox} of PSII, (*B*) Y_{177} of ribonucleotide reductase in mouse, (*C*) Y_{122} of ribonucleotide reductase in *Escherichia coli*.

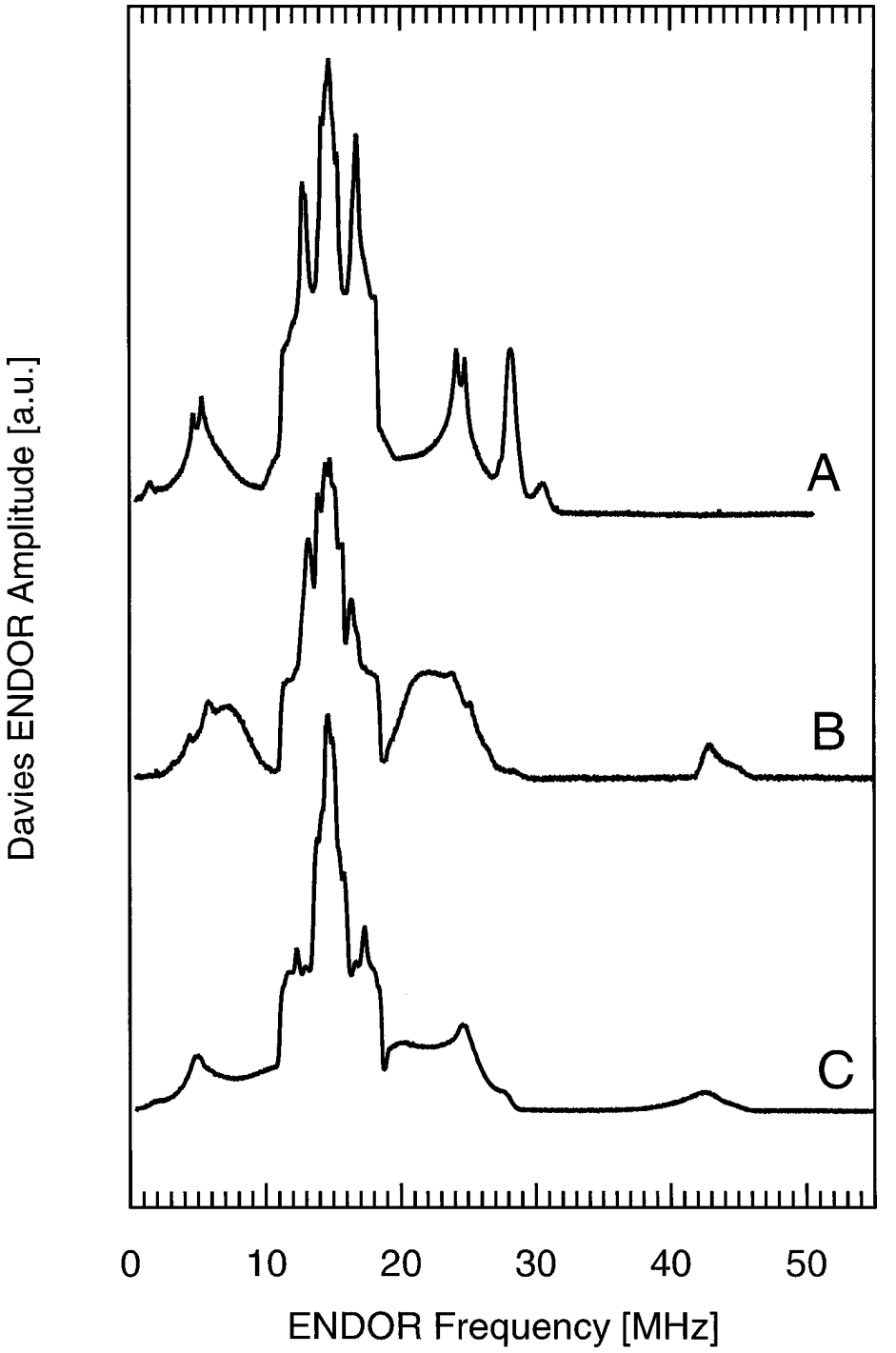

Necessary conditions for the observation of strong modulation effects are (*a*) anisotropic hyperfine or quadrupolar interaction, (*b*) strong MW pulses, and (*c*) cancellation of nuclear splitting for one electronic manifold. Because of condition (*a*) ESEEM effects cannot be directly observed in liquid samples of small molecules. Condition (*b*) means that at least one MW pulse must be strong enough to drive simultaneously an allowed and a forbidden EPR transition (for example $\Psi_1 \leftrightarrow \Psi_3$ and $\Psi_1 \leftrightarrow \Psi_4$). If the transition probabilities of the "allowed" and "forbidden" transition are similar, the ESEEM effect will be most pronounced. This can be achieved by tuning the nuclear level splitting of one electronic manifold by proper choice of the external magnetic field B_0. This is expressed in condition (*c*) and will depend on the nuclear spin and the specific coupling strength (62).

In the 1D ESEEM experiment the two-pulse Hahn echo intensity is monitored as a function of the pulse separation time τ (Figure 2). The oscillation of the echo intensity arises from spins that evolve on different electronic coherences before and after the refocusing pulse (for example coherence $\Psi_1 \leftrightarrow \Psi_3$ in the first time interval τ between the MW pulses and coherence $\Psi_1 \leftrightarrow \Psi_4$ within the second time interval τ after the second MW pulse). Because the respective energy spacings are different for both transitions the refocusing is not 100% but is modulated with the energy difference between the two transitions, which is in fact the nuclear spin–level splitting. In this experiment the modulation can only be observed on a time scale of the transverse electron relaxation time T_2^S, which is in many cases too short to obtain high enough resolution in complex spectra with several coupled nuclei.

A 2D version of the experiment is the stimulated echo pulse sequence, in which both pulse spacing times τ and T are varied (Figure 2). In this experiment nuclear coherence (for example between $\Psi_1 \leftrightarrow \Psi_2$) created by the first two pulses evolves within the time T and is then transferred back into observable electron coherence by the last pulse. In this case the modulation is typically observable on the time scale of the transverse nuclear relaxation time T_2^I, which is often longer than T_2^S but shorter than T_1^S.

In a hyperfine sublevel correlation experiment (HYSCORE) the nuclear coherence within one electronic manifold (for example $\Psi_1 \leftrightarrow \Psi_2$) is transferred by an additional MW pulse into the corresponding nuclear coherence within the other electronic manifold ($\Psi_3 \leftrightarrow \Psi_4$) (63). A 2D-FT leads to a 2D spectrum in frequency space with off-diagonal correlation peaks between hyperfine lines belonging to the same nucleus in both electronic manifolds. This is very helpful in unraveling complex hyperfine spectra with overlapping line contributions from different nuclei.

ESEEM spectra can be analyzed in the time domain as well as in the frequency domain (64). The frequencies in the Fourier transformed ESEEM time traces are the same as in the ENDOR experiment. In contrast, the amplitudes are more complicated functions of spin Hamilton operator parameters (such as hyperfine and quadrupole tensor elements and number of equivalent coupled spins) and experimental parameters (such as MW excitation power, frequency offset, external

magnetic field value, pulse lengths, and dead times). This can be a problem, especially for the assignment of broad anisotropic hfcs in disordered powder samples (61). In disordered samples specific orientations with effective hfcs close to the cancellation condition will be strongly enhanced in the modulation intensity, leading to strong distortions for anisotropic hfc powder patterns. Additionally, blind-spot artifacts for pulse sequences with more than two pulses will modulate the powder pattern lineshape. Alternatively, the modulation depth as well as the damping of the modulation contains additional and independent information on the coupled spin system.

If several nuclei couple to the paramagnetic center, the experimental time trace will be the product of the modulations of the individual nuclei and may become very complex. In order to highlight specific modulations, an isotope-labeling and waveform-division method can be used, as proposed by Mims and coworkers (65, 66). For example, an isotope labeling of ^{12}C ($I = 0$) $\rightarrow$ ^{13}C ($I = 1/2$) results in time traces that are identical, but the isotope labeled time trace is multiplied by the ^{13}C echo modulation. Therefore, a division of the time traces of the two experiments, $^{13}C/^{12}C$, only leaves the specific ^{13}C modulation, if all the other parameters for the sample and experiments are kept constant (67). Although this method is mathematically not exact for disordered powder samples and stimulated echo experiment, as was clearly stated by the authors, it is very successfully applied to disordered protein samples to obtain quantitative information, especially on the number of equivalent nuclei (e.g. water molecules) coupled to the paramagnetic center under investigation.

Nuclei with couplings close to the cancellation condition are strongly enhanced in the ESEEM spectra. Different nuclei can be tuned to this condition by varying the external magnetic field (and thereby the nuclear Zeeman splitting). Therefore, a careful tuning of the MW highlights specific regions of the paramagnetic surrounding (Figure 4). For such nuclei close to the cancellation condition the adiabatic precession of the electron spin in the resulting effective field (external magnetic field plus hyperfine field) under RF irradiation negatively interferes with the excitation field and thereby diminishes the ENDOR effect (65). This shows nicely the complementarities of these two methods. If the modulation depth is small for nuclei not close to the cancellation condition, applying matched pulses can enhance the modulation intensity (68), thereby increasing the sensitivity for such nuclei. This method has not been applied to biological questions yet.

The same groups have often applied ESEEM and pulsed-ENDOR spectroscopy to similar biological systems and paramagnetic centers. Whereas ENDOR investigations concentrated more on the nuclei with higher nuclear Zeeman frequencies, such as ^{1}H, ^{13}C, or ^{31}P, the ESEEM method was mostly used to obtain the complementary information on low frequency nuclei, such as ^{2}H, ^{14}N, and ^{15}N.

A very recent review gives a comprehensive listing of ESEEM spectroscopy applied to metal centers in enzymes and model systems (69). Applications on chromophores in photosynthetic reaction centers have also been reviewed recently (11, 61). Therefore, only a few applications highlighting the potential of ESEEM

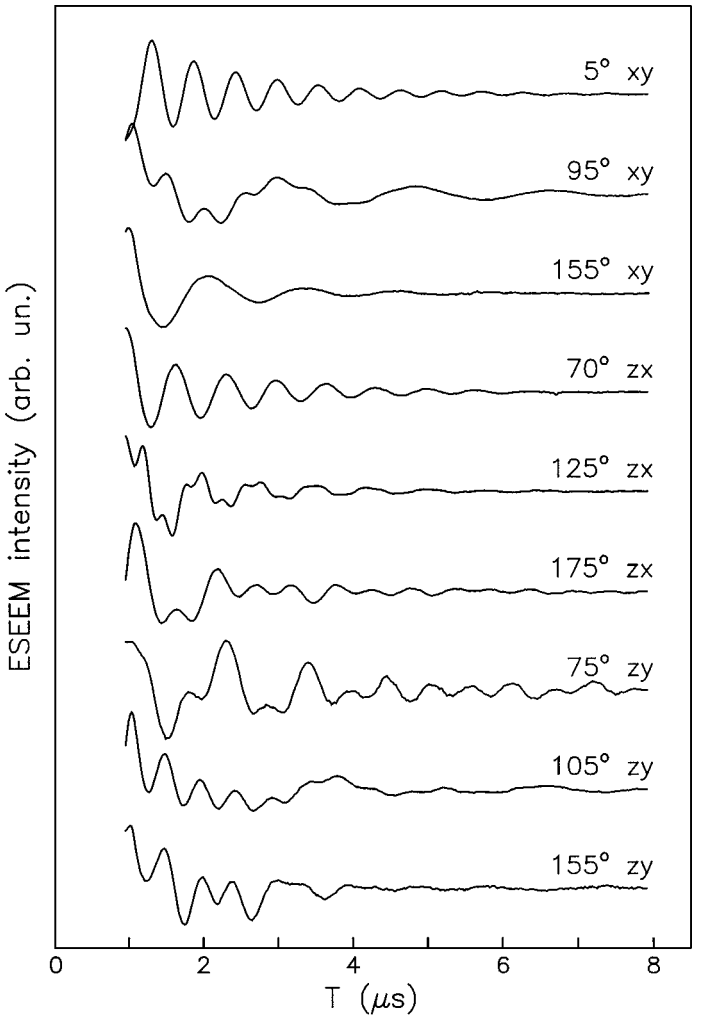

Figure 4 Stimulated echo envelope for a single crystal of azurin. Different orientations of the magnetic field with respect to the g-tensor principal axis system are shown. The decay of the echo intensity has been removed to emphasize the modulation-frequency dependence on the crystal orientation [Reprinted with permission from (80).]

spectroscopy for the investigation of the local structure of paramagnetic centers will be described here in more detail.

Cu^{2+}-metal centers ($S = 1/2$, $I = 3/2$) in enzymes have been extensively studied by ESEEM methods. One of the first ESEEM applications on biological systems was done on the Cu^{2+}-center in stellacyanin (70). For the ^{14}N-nucleus close to cancellation the quadrupole tensor $\hat{Q}$ can be determined by analyzing

the echo modulation. Comparison of the data obtained in these experiments with those from model systems and nuclear quadrupole resonance data allows the identification of the ligating molecule (mostly histidine), the ligand positions and orientations, and also the protonation of the nitrogens (72, 73, 246). Two to four histidine ligands were detected by ESEEM spectroscopy for different Cu^{2+}-proteins by comparison of the experimental ESEEM time traces with simulations (74–79). Multifrequency ESEEM is especially helpful for tuning different nitrogens with distinguishable hfcs to the cancellation condition. Whereas at X-band frequency the ESEEM experiment is especially sensitive to the remote imidazole nitrogen, the situation is different at higher frequencies. With W-band ESEEM experiments the directly ligated nitrogen of the imidazole ring in the blue copper protein azurin has been observed in single crystal studies (80) (Figure 4), whereas X-band ESEEM detected the remote nitrogens (81, 82). Isotope labeling ($^{1}H/^{2}H$ or $^{12}C/^{13}C$) and the spectra division method were used to obtain quantitative information about other ligands of the Cu^{2+}-ion, such as water molecules (67, 83–86). The replacement of a histidine nitrogen ligand by the enzyme inhibitor cyanide was proven in superoxide dismutase by isotope-labeled ($^{14}N/^{15}N$) CN^{-} (87) and the replacement of a water ligand by N_3^{-} in laccase (88). Recently, Cu^{2+} was used to replace nonheme Fe^{2+} in bRC and in a dioxygenase. The histidine couplings observed on the Cu-ESEEM spectra were used to identify possible ligands to the native Fe^{2+}-ion (89, 90).

Mn^{2+} is another metal ion that was investigated by ESEEM spectroscopy in several protein complexes. In many cases Mn^{2+} can substitute for other naturally abundant metal ions, as for example the diamagnetic Mg^{2+}-ion, and can therefore serve as a paramagnetic probe in the investigation of these metal sites. The analysis of field swept spectra and the quantitative analysis of ESEEM experiments is rather complicated (91), owing to the high spin state ($S = 5/2, I = 5/2$), the large manganese hfc ($\sim$9 mT), and the zero field splitting tensor (typically coupling strengths D of 10–100 mT). Because of the high spin state, the different allowed and forbidden electronic transitions overlap, leading to complicated EPR and ENDOR spectra. In principle, pulsed experiments will allow these different transitions to be distinguished by their transition moments (92), but this has been used only recently to simplify such spectra (93). Nevertheless, quantitative information on the ligand sphere could be obtained by either isotope exchange of the water solvent (e.g. $^{2}H_2O$ or $H_2{}^{17}O$) or isotope labeling of specific amino acids ($^{14}N/^{15}N$, ^{13}C, ^{17}O, ^{2}H). This allowed the determination of the number of water ligands (94) and the identification of the peptide ligands (95). What can be achieved by ESEEM spectroscopy on such a metal center in a protein complex was demonstrated very impressively on the $p21^{ras.}$ Mn·GppNHp complex (96, 97). Mn^{2+} replaced the natural diamagnetic Mg^{2+}-ion in this complex for the EPR investigations. By specific mutations of amino acids in the close neighborhood of the metal center (^{15}N-Ser17, $^{2}H/^{13}C/^{15}N$-Thr35, ^{13}C-Asp57) and by detailed analysis and simulation of the high spin ESEEM effects (91) an EPR structure of the metal site (up to 0.5 nm) could be obtained in good agreement with X-ray results (98). In the same way the metal binding sites

of isolated F1-ATPase from spinach chloroplasts and from *Bacillus PS3* have been studied by ESEEM spectroscopy using Mn^{2+} (99, 100) or vanadium (101, 102) as a paramagnetic substitute for Mg^{2+} and Ca^{2+}. The protein and ATP nucleotide binding ligands to the metal ion and the change in the metal binding site upon addition of ATP have been identified by EPR spectroscopy. In cytochrome *c* oxidase ESEEM spectroscopy was used to identify the amino acid ligands of the Mn^{2+}-site, which does not participate in the electron transfer reaction but occurs naturally in several organisms (103). In a recent work $^{14}N/^{15}N$ and $^{1}H_2O/^{2}H_2O$ ESEEM experiments have been used to identify the interaction of Mn^{2+}-ions with guanosine in the hammerhead ribozyme complex (104).

Multifrequency ESEEM, ranging from S-band (3 GHz) to P-band (15 GHz), was used to distinguish different states of Mo^{5+} ($S = 1/2$) in molybdoenzymes such as xanthine or sulfide oxidase. Additionally, their ligation sphere and geometry was postulated on the basis of these EPR and EXAFS measurements (105–109).

Photosynthetic proteins have been intensively and competitively examined by ESEEM spectroscopy. The electron spin density distribution on the primary electron donor $P^{+\bullet}$, a chlorophyll dimer, was intensively studied by nitrogen 1D stimulated echo and 2D HYSCORE experiments (61, 110–112). Complementary to ENDOR investigations, ESEEM experiments were used for the different quinone acceptors to detect hfcs of nitrogens in amino acid residues. Recent publications have appeared on the electron acceptor $A_1^{-\bullet}$ of PSI (113), on $Q_A^{-\bullet}$ in bRCs (114–116), on $Q_A^{-\bullet}$ in PSII (117) (attempting to resolve some earlier controversial results), and on $Q_H^{-\bullet}$ in quinol oxidase (118). In PSII the tyrosyl radical $Y_D^{-\bullet}$ was investigated by $^{1}H/^{2}H$ ESEEM (119, 120), the manganese cluster (121–126), and very recently, the carotene cation radical (127), in which a close-by tryptophan residue was assigned.

Further HYSCORE spectroscopy has been done to analyze nitrogen and proton/deuteron hfcs of flavin radicals in ferredoxin-$NADP^+$ reductase and in flavodoxin (26, 128). In the proteins amine oxidase and methylamine dehydrogenase intermediate substrate radicals within the catalytic cycle could be analyzed by ESEEM spectroscopy (129–131). A recent HYSCORE experiment on the bound quinone $Q_H^{-\bullet}$ in quinol oxidase is shown in Figure 5. The obtained nitrogen quadrupole tensor Q shows that the semiquinone is most strongly coupled to a nitrogen nucleus of the protein backbone (118).

Pulsed Electron Double Resonance (PELDOR)

Because the interaction of two electron spins with each other is formally identical to the interaction of an electron spin with a nuclear spin (see Equation 1 and Figure 1), the conceptual principles of pulse methods to observe small magnetic dipolar couplings between distant paramagnetic centers are very similar to the ESEEM experiment. PELDOR experiments (132), also called double electron electron resonance (DEER) (133), have been used to measure interactions between radicals for distances of up to 5 nm (134, 135). For this method two different MW

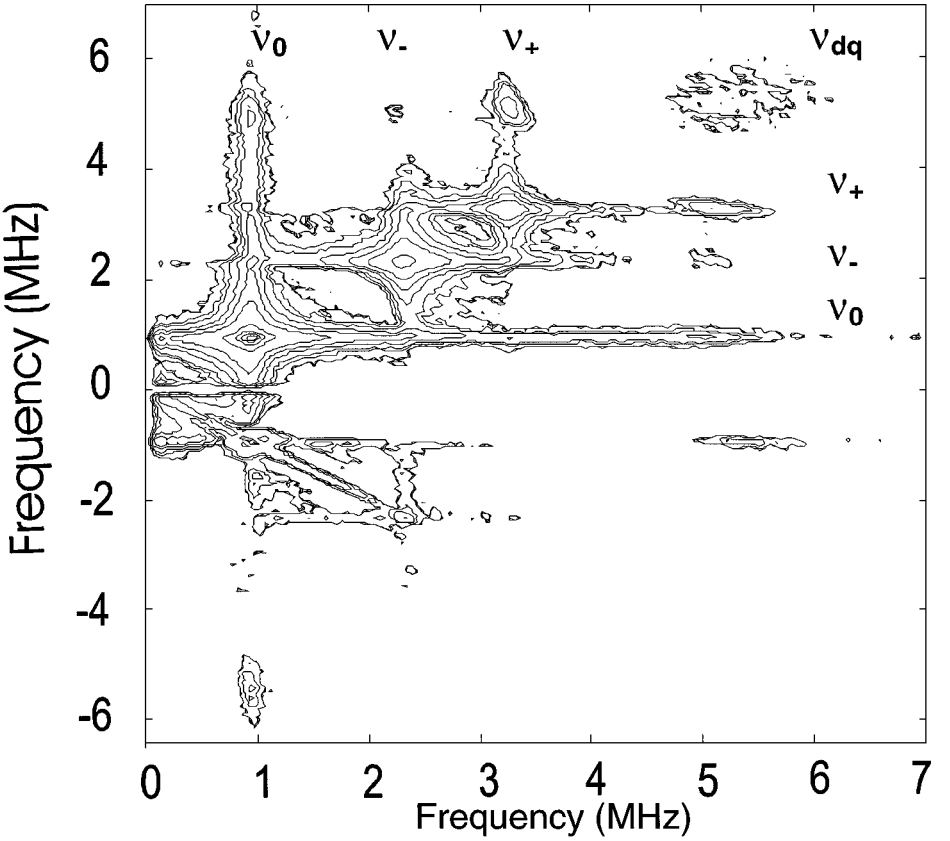

Figure 5 X-band HYSCORE spectra of the semiquinone $Q_H^{-\bullet}$ of bo_3 ubiquinol oxidase from *E. coli* after echo decay subtraction and magnitude Fourier transformation of the 2D time traces. The correlation peaks of the three quadrupolar split levels (ν_0, ν_-, ν_+) of the α electronic manifold with the double quantum peak (ν_d) of the β electronic manifold are well resolved (118).

frequencies (ω_a in resonance with electron spin A and ω_b in resonance with electron spin B; see Figure 2) have to be applied to the sample via the MW resonator. An example of a new four-pulse version of this experiment applied to two biradical model systems (with interspin distances of 1.9 and 2.8 nm) is shown in Figure 6, in which the dipolar oscillations, containing the distance information, are easily observable (135). Instead of a pulsed excitation with two distinct MW frequencies, the magnetic field can be jumped between pulses to get into resonance condition with the second paramagnetic species (136, 137). If the spectra of the two paramagnetic centers overlap, the experiment can also be performed with a single MW frequency; this is the so-called $2 + 1$ pulse sequence (138, 139). In this experiment care has to be taken to distinguish the dipolar coupling of the two paramagnetic centers from

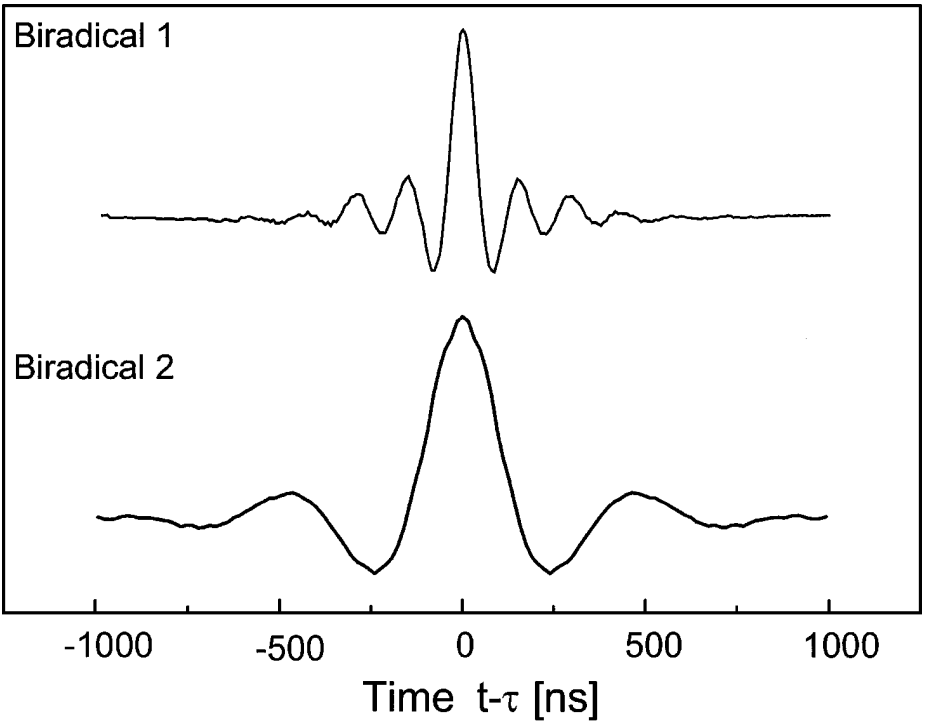

Figure 6 Four-pulse double electron electron resonance time domain signal on two biradical model systems after subtraction of the background signal owing to intermolecular interactions. From the oscillations an electron-electron distance of 1.94 ± 0.05 nm for biradical 1 (upper trace) and of 2.83 ± 0.05 nm for biradical 2 (lower trace) could be determined. [Adapted with permission from (135).]

hfc to nuclei, as observed by ESEEM (140). Another pulse scheme, the DQ 2D-EPR experiment (141), is a direct EPR analogue of a classical nuclear magnetic resonance (NMR) double quantum coherence experiment, and was demonstrated on a nitroxide biradical sample with an interspin distance of 3 nm (142).

The possibility of measuring long distances with pulsed-EPR methods is extremely attractive, especially for biological samples. It can be used to identify electron transfer pathways in proteins and measure the distances and relative orientations of the involved centers. In combination with site-specific double-spin labeling techniques it will allow the determination of long range structural constraints of the protein backbone and information on conformational mobility in specific loop regions. A more comprehensive overview of cw-EPR, PELDOR, and pulsed-EPR relaxation methods to measure distances between paramagnetic centers and some first applications will appear soon (143).

An early application of the "2 + 1" pulse method to biological systems was the measurements of the distance between two spin-labeled cysteine residues of a hemoglobin tetramer (139). The measured distance of 3.5 ± 0.15 nm was in good agreement with the X-ray structure. PELDOR and the "2 + 1" pulse sequence were used to measure the distances between the tyrosine radicals $Y_D^{\bullet}$ and $Y_Z^{\bullet}$, the semiquinone radical $Q_A^{-\bullet}$, and the Mn_4-cluster in PSII samples (144–146). Distances of up to 4 nm and relative orientations have been determined between the different chromophores. Together with pulsed-EPR relaxation measurements, out-of-phase-echo measurements (both described in the next two sections), and cw-EPR power saturation measurements, these data allowed prediction of a skeleton of the chromophore locations within the protein complex. Very recently, an application of the four-pulse double electron electron resonance experiment (135) was performed in double spin-labeled human carbonic anhydrase II to measure distances and mobility in the range of 2 nm (147).

Pulsed EPR/Relaxation Measurements

If one of the two paramagnetic species is a fast relaxing species, as for example a metal center, the PELDOR method will not be applicable anymore. However, information on the interspin distance can be gained by measuring the relaxation enhancement on the slowly relaxing paramagnetic species, caused by the dipolar coupling to the fast relaxing species (148). Usually the relaxation behavior of a paramagnetic center will be a complex temperature-dependent process with contributions from different physical mechanisms. Therefore, to obtain a quantitative value for the interspin distance, the relaxation rates of both paramagnetic species without the dipolar coupling but otherwise identical conditions have to be known. This is difficult to achieve in biological samples, but often model systems for the slowly relaxing species are used to obtain their unperturbed rates. In some proteins one of the paramagnetic species can be switched into a diamagnetic state. The rates of the fast relaxing species will not be perturbed by the dipolar coupling but are often difficult to measure.

Applications of these pulsed-EPR techniques to determine interspin distances in biological samples have been demonstrated most impressively in PSII samples. Already, changes of the relaxation time T_1 of the tyrosine radical $Y_D^{\bullet}$ depending on the redox state of the Mn_4-cluster have been interpreted as arising from the dipolar coupling of the two paramagnetic species (149). Thereafter, distances between the Mn_4-cluster (or for Mn_4-cluster-depleted samples to the Fe^{+2} ion) and the paramagnetic species $Y_D^{\bullet}$, $Y_Z^{\bullet}$ $P_{680}{}^{+\bullet}$, $Chl_Z{}^{+\bullet}$, and $Pheo^{-\bullet}$ were estimated by saturation recovery relaxation measurements (150–154). Similar to the PSII experiments, the coupling of the tyrosyl radical $Y_{122}^{\bullet}$ with the diferric center in ribonucleotide reductase was also detected by saturation recovery experiments (155).

A variant of this method is the hole-burning method (156), in which a selective excitation hole is burned into the inhomogeneous broadened EPR line, and the

broadening of the hole by relaxation effects is studied. This method was applied to PSII and PSI chromophores to measure distances (157, 158).

Other examples for the use of this relaxation experiment are measurements on spin-labeled methemoglobin and methmyoglobin, in which different nitroxide spin-label to heme-iron distances (in the range of 1.5–3 nm) were determined (159, 160).

A different relaxation source for paramagnetic centers beside dipolar coupling to fast relaxing electron or nuclear spins is the motional modulation of the Larmor resonance frequency by orientation-dependent anisotropic interactions, as determined by the hfc or the g-tensor. In this case the measurement of the relaxation times over the whole spectral width allow determination of not only information on the rotational correlation time τ_c of the molecule but also detailed information on the type of motion the molecule undertakes. In proteins this motion of a bound nitroxide spin label is non-Brownian and hindered, depending on the specific position of the spin label. Therefore, these measurements can help obtain detailed information not only on the molecule itself, but also on the protein backbone. The time windows of motional processes observable on spin labels by cw-EPR have been drastically extended by cw-saturation-transfer-EPR (161) and pulsed EPR methods, such as saturation recovery EPR and 2D-electron-spin-echo (2D-ESE) spectroscopy (162, 163). Whereas the very slow motional region (with correlation times of up to 1 ms) can be detected by saturation-transfer–EPR (164, 165), pulsed EPR allows investigation of motional processes lying in the correlation time range between ns and several hundred μs. ESE spectroscopy is one of the basic tools that allows probing of slow molecular motions of spin labels, for example in membrane model systems (166, 167). Furthermore, the examination of molecular motions can be done by 2D-FT EPR; a comprehensive treatment including descriptions of free induction decay–based correlation spectroscopy (COSY) and spin echo correlation spectroscopy (SECSY) can be found in (168).

Characterizing protein-protein and protein-lipid interactions by observation of changes in rotational diffusion of the spin labels involved requires the use of comprehensive mathematical and rotational diffusion models (169–172). As mentioned above, application of pulsed-EPR techniques simplifies the interpretation by distinct separation of time-dependent and static-spin Hamiltonian parameters.

An early investigation of echo-detected motional dynamics was performed on a maleimide spin-labeled deoxygenated hemoglobin, in which the motion of the polymerized molecule could be differentiated from monomeric molecules in solution under physiological conditions (173). Most recently, this method has been used for probing temperature-dependent librational motion in glass formed from the intracellular medium at low temperature in seed and pollen. Correlation between the water content in *Typha latifolia* pollen and the librational motion of the spin label in the cytoplasma could be shown (174). Echo-detected EPR has further been used to characterize the molecular motion of the cholestane spin label in a multibilayer in the gel phase (167). With a model of uniaxial

librations, the projection angle of the libration axis in the molecular plane was determined relative to the N–O bond direction of the spin label. Motional states of spin labels were also characterized with pulsed-EPR in cardiolipin-cytochrome *c* bilayers (175) and in spin-labeled Ca^{2+}-ATPase in the sarcoplasmatic reticulum membrane (176). Interactions of stearic acid spin-label pairs in multilamellar liposomal dispersions were characterized with saturation recovery-EPR methods and by measurements of the spin lattice relaxation time T_1 (177). Site-specific spin labeling and pulsed-EPR techniques have been used to characterize melittin at membrane surfaces (178), most recently using pulsed high-field (HF)-EPR on bacteriorhodopsin (179). Thereby, different modes of molecular motions were characterized in dependence on the position of the spin label. Pulsed-HF-EPR allows these investigations to be extended to other classes of molecules, such as organic radicals with only small anisotropic hfc and g-tensors, which are not resolved at X-band frequencies. At high fields these radicals' g-tensor anisotropy can be resolved (as described below), and the contribution of this tensor to the motional relaxation will be strongly enhanced (180). W-band pulsed-EPR experiments were used to investigate the librational motion of the semiquinone $Q_A^{-\bullet}$ in bRC (181). The uniaxial librational motion of the protein-bound semiquinone along the C-O axis (in contrast to the more isotropic Brownian tumbling of semiquinone in frozen solution) could clearly be resolved by the 2D-ESE experiments (Figure 7).

Transient EPR/Correlated Radical Pairs

Photosynthetic proteins (especially bRC in which high resolved X-ray structures are available) have not only been extensively studied with all sorts of advanced EPR methods, but have also helped in the development of new methods and concepts of EPR spectroscopy (182, 183).

Transient EPR methods, first developed for the detection of photo-excited transient triplet states of aromatic molecules (184), have been used extremely successfully to obtain unique information on the distances and relative orientations of the chromophores involved in the fast electron-transfer reaction in photosynthetic proteins. In these proteins a fast electron transfer reaction is initiated by photoexcitation, leading to a transient radical pair of an electron donor molecule $P^{+\bullet}$ and an electron acceptor molecule $Q^{-\bullet}$ on a sub-ns time scale. Because the electron transfer reaction is started from the excited singlet state of the primary donor $^1P^*$, the population of the dipolar coupled radical pair energy levels (see Figure 1*b*) does not obey Boltzmann distribution law. Instead, only the Ψ_2 and Ψ_3 levels are selectively populated via intersystem crossing, which leads to an

Figure 7 Two-dimensional-electron-spa-echo (2D-ESE) (W-band) experiments on ubisemiquinone radical in frozen isopropanol solution (upper trace) and in bRC (lower trace). Both measurements were performed at 120 K. The anisotropy of the relaxation time T_2 within the powder spectra is clearly visible and very different for the two environments.

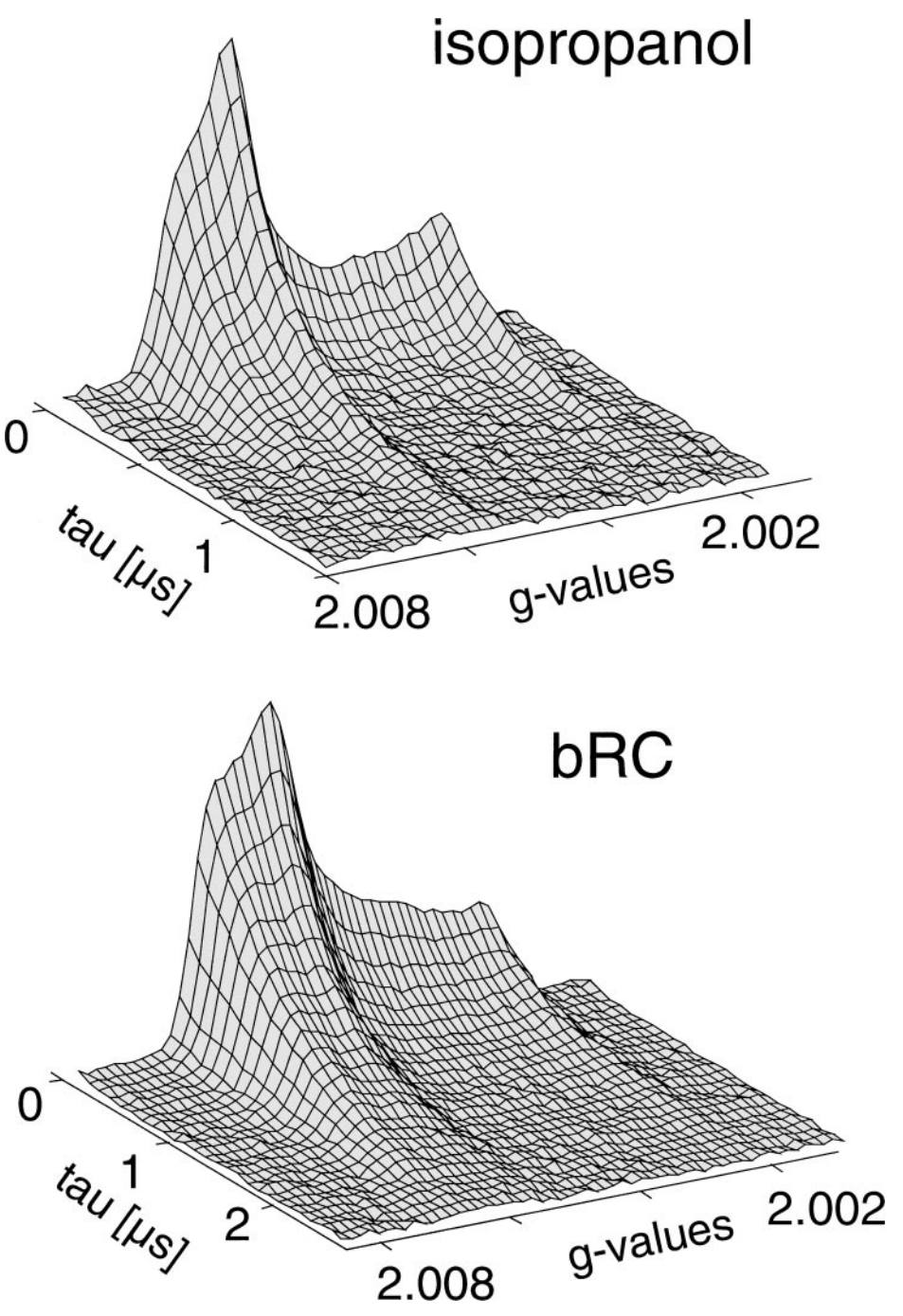

unusual spin polarization, described as longitudinal two-spin order, resulting in the specific features of the EPR signals.

These EPR spectra, detected as time-resolved MW responses directly after the laser flash, are therefore highly spin polarized with emissive and absorptive components. The first applications of the transient EPR method to biological systems were performed on bRC (185). The spin polarized correlated radical pair transient was recorded for different resonant field values B_0 and could be used to deduce the relative orientation and, to some extent, the distance of the dipolar-coupled radical pair $P^{+\bullet}$-$Q^{-\bullet}$ (183, 186, 187). High-field two-pulse echo-detected polarized spectra were used to get enhanced information on the relative orientation of the $P_{865}{}^{+\bullet}$-$Q_A{}^{-\bullet}$ pair in bRC (188) and on the pair $P_{700}{}^{+\bullet}$-$A_1{}^{-\bullet}$ in PSI (189) because the anisotropy of the semiquinone g-tensor could be resolved at such field values (3.4 T).

In addition to the nonthermal polarization created by the photo-induced electron transfer, zero-quantum coherence between the charge-separated spin states is created, which are (because of the dipolar and exchange coupling) not eigenstates of the coupled radical pair. Because of the large distance of the two radicals ($\sim$2 nm) and the fast electron transfer ($<$1 ns), coherence between the populated states Ψ_2 and Ψ_3 exists after a short laser pulse excitation. This was theoretically predicted (190) and experimentally observed for short delay times after the laser flash PSI (191). The coherent quantum beat signals, observed as a function of the magnetic field position, could be used to obtain detailed structural information on the radical pair (192). Finally, the unusual out-of-phase-echo signal (193) (observed in phase with respect to the excitation pulses) of this coupled radical pair can be used to measure with high accuracy the distance between the two paramagnetic species because the echo amplitude is periodically modulated as a function of the pulse separation time τ (see Figure 2) by the dipolar (and exchange) interaction (194–196). This method is just as sensitive to distances as the more complicated PELDOR or double quantum experiments and has been used to measure the distances between the different cofactors in bRC, PSI, and PSII with high accuracy (182, 197–205). Changes of these distances in light-adapted frozen samples were also investigated by these methods (206, 207). Figure 8 shows the Fourier transformations of time traces obtained from the radical pair $P_{865}{}^{+\bullet}$-$Q_A{}^{-\bullet}$ of bRC and from $P_{700}{}^{+\bullet}$-$A_1{}^{-\bullet}$ in PSI. The distances of 2.82 nm and 2.54 nm could be deduced by simulations (dotted lines) (202). Finally, it has also been shown theoretically (208) as well as experimentally in bRC (209) that double quantum coherences can be created under these specific starting conditions by just a single MW pulse.

High-Field/High-Frequency EPR

As can be seen from the first term of the spin Hamiltonian (Equation 1), the electron Zeeman splitting scales linearly with the magnetic field B_0. In first order, an increase of B_0 requires an equivalent increase of the Larmor frequency ν_{MW}. This applies for cases in which a particular spin system is studied at different magnetic

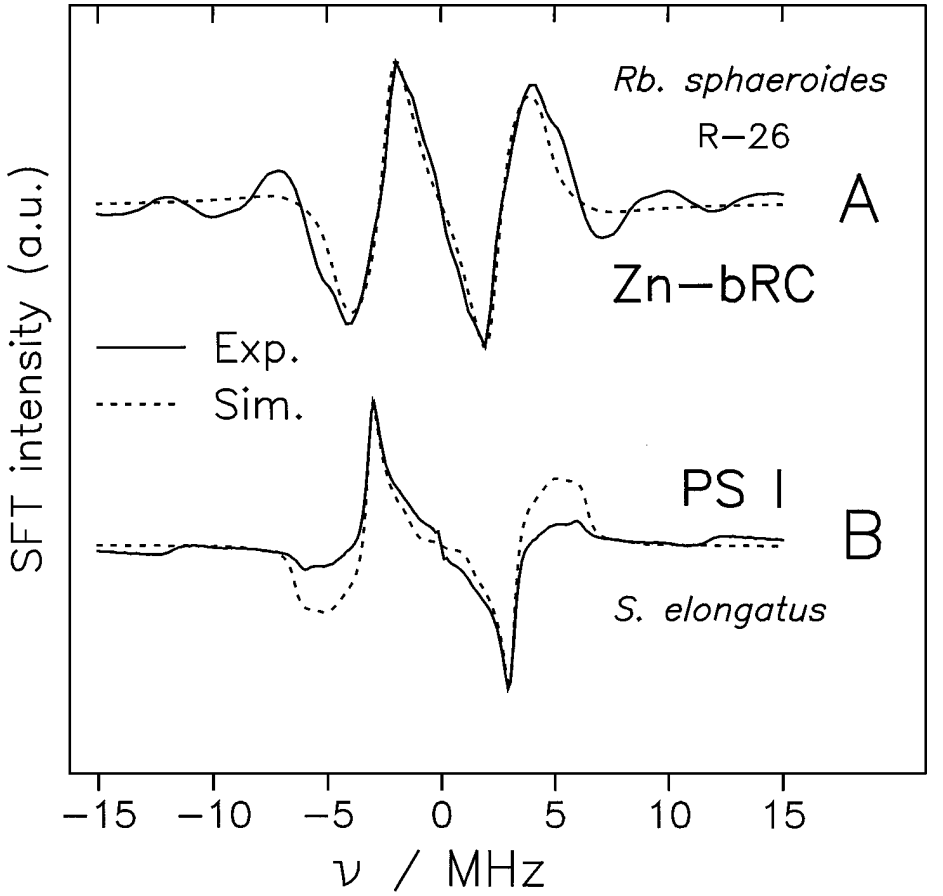

Figure 8 Sine Fourier transforms of the out-of-phase echo modulation for the radical pair $P_{865}^{+\bullet}$-$Q_A^{-\bullet}$ of bRC and the pair $P_{700}^{+\bullet}$-$A_1^{-\bullet}$ of PSI. The dead time of the traces was reconstructed with maximum entropy methods. The simulations (dotted lines) of the experimental patterns yield 2.84 ± 0.03 nm for the distance in bRC and 2.54 ± 0.03 nm in PSI. A small exchange coupling of $J = 1\ \mu$T was obtained for both systems. [Adapted with permission from (182).]

fields if there are no additional field-dependent parameters. Consequently, "high-field EPR" and "high-frequency EPR" are effectively synonyms in most cases.

In principle, the motivation for HF-EPR is the same as for the comparable development in NMR. As in NMR at increasing Zeeman energy, the spectral resolution increases in most cases and the population difference or polarization of the spin states (α and β) increases according to the Boltzmann distribution as well. This leads, together with the higher quantum energy of the observed transitions, to higher sensitivity of HF-EPR experiments. Besides these very basic motifs,

HF-EPR opens new frontiers for systems with large zero field splitting, which may be totally EPR-silent at normal EPR frequencies (210), and for systems with very small g anisotropies and unresolved hfcs, as in many aromatic organic radicals (211–217).

In HF-EPR the magnetic field is usually higher than 2 Tesla and thus requires, typically, the use of a superconducting magnet. The first corresponding frequency band is called W-band and ranges from 70–110 GHz. Many technical requirements substantially change for such high-MW frequencies close or above the limit for conventional semiconductor MW technology. "Classical" spectrometer designs with a MW resonator in reflection mode and using commercial MW components such as a waveguide MW circulator can still be realized at frequencies up to approximately 140 GHz (D-band) (1, 218–221). At higher frequencies the small wavelengths become prohibitive for the effective operation of rectangular waveguides, and quasi-optical methods have to be used to replace classical MW components. By using such techniques, or by combining them with classical MW components, sensitive cw spectrometers can be built at frequencies even in the low-mm and in the sub-mm range (222–224).

Cw HF-EPR was first developed by the group of Y Lebedev in Moscow (225), who used a MW frequency of 140 GHz. The first pulsed HF-EPR setups were built in Leiden (226), followed by spectrometers in Moscow (218), at MIT (227), and in Berlin (228) at W-band or D-band frequencies. By using pulsed far-infrared lasers, pulsed EPR was demonstrated at 604 GHz in Grenoble (229, 230). Since 1996, HF-EPR instrumentation at W-band has been offered commercially by Bruker Analytik (1) for cw experiments as well as pulsed-EPR experiments.

When half-integer high-spin systems ($S > {}^1\!/_2$) are studied, the linewidth of the central EPR transition ($m_S = +{}^1\!/_2$ to $m_S = -{}^1\!/_2$) is broadened by higher order zero field splitting contributions. Because of the inverse field dependency of these contributions, HF-EPR often leads to narrower lines and thus to increased information content for small interactions such as hfc of ligands (231–233) or dipolar coupling to other paramagnetic centers (234). The spectral resolution for systems with large hfc is often further increased as a result of the suppression of forbidden m_I transitions at higher field values. Finally, as already mentioned above, systems with very large zero field splitting (in the order of the electron Zeeman splitting) even become EPR-silent at low field values (210).

As a result of the increased Boltzmann spin polarization, magnetic resonance experiments become more sensitive at higher fields. However, this effect is partially compensated by technical restrictions, limiting the performance of many MW components at the smaller wavelengths (180). Another reason for the drastic increase in absolute sensitivity (in spins/mT) is found for HF-EPR spectrometers utilizing a MW-resonator. Owing to the smaller wavelength, the resonator dimensions decrease, leading to smaller sample volumes ($<1\ \mu$l) with still high filling factors (219, 220, 228). For simple transmission mode setups without resonator (217, 235, 236), the latter argument does not apply. Instead, the concentration

sensitivity (in spin/mT/cm^3) has to be considered in this case because large sample volumes (several hundred μl) can and must be used. Despite this, cw-EPR experiments can be performed quite successfully in broadband setups without resonators. Alternatively, for pulsed HF-EPR the incorporation of a MW resonator, preferably in the reflective operation mode, is indispensable because of the limited MW power available. The bandwidth of the MW resonator is broad enough to support the MW pulses even for optimal large Q values at high MW frequencies (whereas the Q value and therefore the sensitivity has to be lowered drastically in the case of pulsed X-band EPR applications). This leads to good conversion factors for the MW B_1-field, a short ringing and dead time after the pulses, and a high sensitivity (228).

The performance of ENDOR and related double resonance experiments at high magnetic fields offers additional specific advantages, for example for studying organic radicals with small g-anisotropies: The improved spectral resolution obtained in the EPR dimension allows one to record orientation-selective ENDOR spectra and thereby to improve the information content of ENDOR spectroscopy on powder-type samples with randomly oriented radicals (14, 30, 237). Another significant advantage of HF-ENDOR is the increased nuclear Zeeman interaction, which separates the free nuclear Larmor frequencies of different nuclei and thereby enhances the spectral resolution in the NMR dimension. Accordingly, spectral overlap can be reduced and spectra can be simplified (39, 238). Considerable simplifications of ENDOR spectra are also observed owing to the increased ratio of nuclear Zeeman frequency/hfc, as pointed out above. In analogy to the advantages of HF-EPR on metalloproteins, contributions of higher m_S-transitions are suppressed in the HF-ENDOR experiments as well (239). Furthermore, the advantages of HF-ENDOR can be combined with those of pulsed TRIPLE resonance methods (240). Thereby, spectral assignments of different nuclei and metal centers can be mapped in 2D spectra (241).

Applications of pulsed HF-EPR in biological systems are mentioned and cited above. Whereas ESEEM spectroscopy at high magnetic fields is limited to few nuclei with specific hfc (228, 242), the application of pulsed HF-ENDOR (220, 228, 237) and HF-2D-ESE (228) offers several advantages, as mentioned above. First, applications to biological systems include the W-band ESEEM spectroscopy on the direct coordinated histidine ligands (80, 243) (Figure 4) and W-band ENDOR spectroscopy on two remote histidine nitrogens and three distant protein backbone nitrogens (238) in small single-crystal azurin samples. The ubisemiquinone $Q_A{}^{-\bullet}$ in bRC was investigated by pulsed W-band ENDOR (14), 2D-ESE (181) and transient EPR (188) experiments. The relative orientation of the quinone molecule with respect to the bacteriochlorophyll donor molecule $P_{865}{}^{+\bullet}$, its hydrogen bonding to the protein and its uniaxial librational mobility in the protein pocket could be deduced from these experiments. Similar transient W-band EPR experiments were performed on the correlated radical pair $P_{700}{}^{+\bullet}$-$A_1{}^{-\bullet}$ in PSI samples (189). Other applications of W-band pulsed ENDOR are the determination of nitrogen and proton hfcs to the Cu_A center in cytochrome *c* oxidase (39) and to the Mn^{2+}-ion in

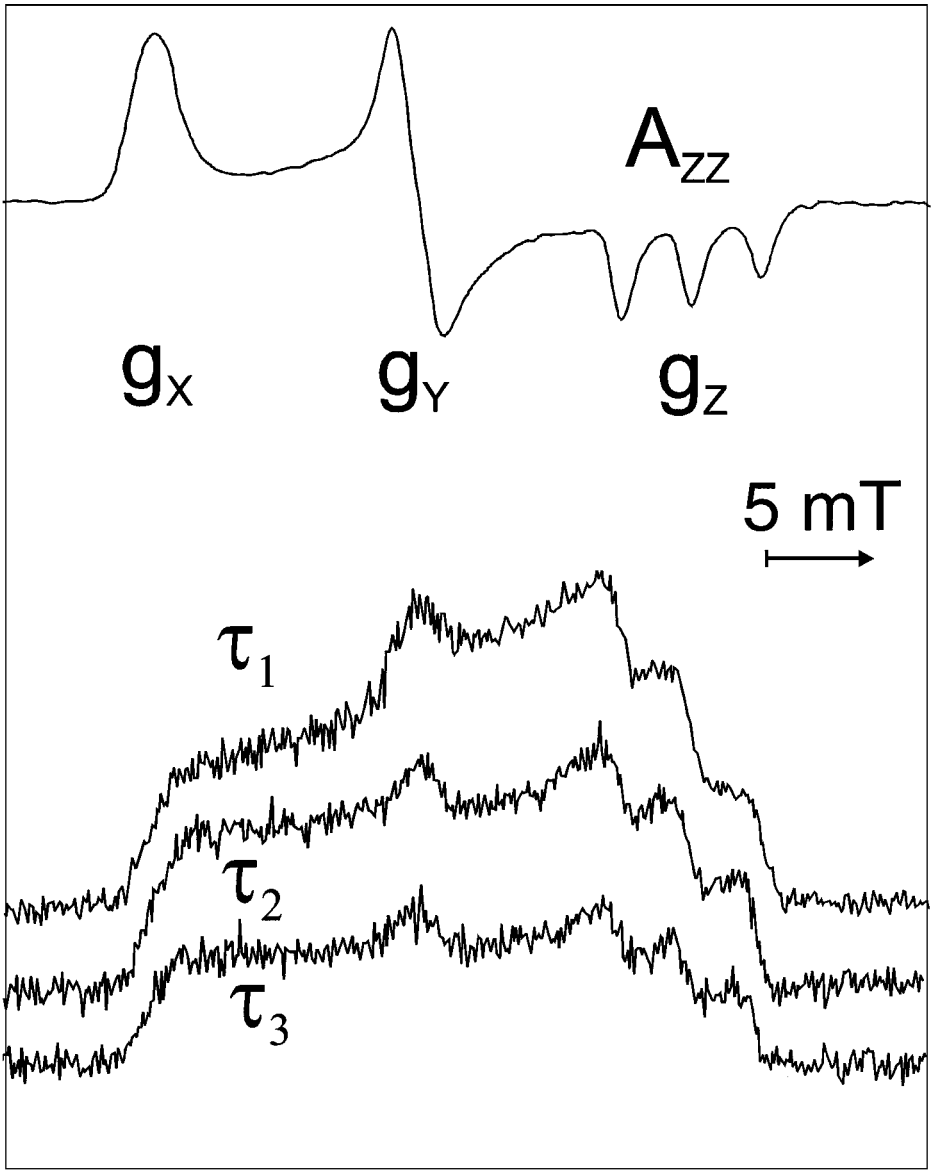

Figure 9 Field swept two-pulse echo spectrum of TEMPO spinlabel in a polystyrene matrix at 180 GHz MW frequency. In the cw spectra (upper trace) the well-resolved canonical peaks of the anisotropic g-tensor and the resolved nitrogen hfc A_{zz} component can be easily seen. The echo-detected spectra recorded for different τ values ($\tau_1 = 100$ ns, $\tau_2 = 200$ ns, $\tau_3 = 400$ ns) show the anisotropic T_2 relaxation time.

concavalin A (43) and the determination of the tyrosine radical in ribonucleotide reductase (30). Field-swept echo-detected D-band (140 GHz) EPR spectra of the apogalactose oxidase tyrosyl radical at low temperatures showed an increased hfc resolution compared to the saturation-broadened cw-EPR spectrum (244). In a recent publication first W-band field-swept echo experiments for the investigation of motional dynamics of nitroxide spin-labeled bacteriorhodopsin at the dynamic glass transition temperature were presented (179). The anisotropic transverse relaxation time T_2, measured over the whole powder pattern, can be used to analyze this motion in detail. An example of such an experiment, performed on our home-built pulsed 180 GHz EPR spectrometer (245), on a nitroxide spinlabel in polystyrene sample is shown in Figure 9. At these high magnetic fields (6.4 T) the anisotropic g-tensor is well resolved and dominates the spectra, in contrast to X-band frequencies in which the anisotropic nitrogen hfc tensor is dominant. Therefore, by HF-EPR orientational selection can be observed along g_x, g_y, and g_z, whereas at X-band only the z orientation is well resolved. The differences of the relaxation times T_2 for the different g-values can be seen by the change of the relative spectral intensities for different pulse separation times τ the well.

OUTLOOK

Pulsed-EPR and ENDOR methods extend the possibilities of cw-EPR to extract structural information from paramagnetic centers. This is especially true for disordered biological samples with several spectral overlapping paramagnetic species. The basic pulse sequences and experiments designed to unravel complex systems as described in this review have been developed and calibrated on model systems. As can be seen, they have been already successfully applied to study the local structure of some paramagnetic centers in biological systems. Their use in biological systems will, to our belief, further increase in the near future. One of the main reasons for this is that molecular quantum theoretical calculations have rapidly improved and the link from EPR spectroscopic data to a molecular structure will be much more direct in the future.

ACKNOWLEDGMENTS

We are indebted to all members of our group for their helpful suggestions and assistance in preparing the manuscript, especially Hildegard Mathis for getting the references in the correct order. Furthermore, we would like to thank all the authors who agreed to contribute a figure from their own research work to this review, especially Wolfgang Lubitz, who contributed unpublished work performed in his laboratory (Figure 3). Financial support of our work by the Deutsche Forschungsgemeinschaft (SFB472 and SP HF-EPR), the county of Hesse and the Fond der Chemischen Industrie is gratefully acknowledged.

LITERATURE CITED

1. Höfer P, Maresch GG, Schmalbein D, Holczer K. 1996. *Bruker Rep.* 142:15–21
2. Poole CP, Farach HA. 1972. *The Theory of Magnetic Resonance*. New York: Wiley
3. Feher G. 1956. *Phys. Rev.* 103:834–35
4. Mims WB. 1965. *Proc. R. Soc. A* 283:452
5. Davies ER. 1972. *Phys. Lett.* 47a:1–2
6. Grupp A, Mehring M. 1990. In *Modern Pulsed and Continuous Wave Electron Spin Spectroscopy*, ed. L Kevan, MK Bowman, pp. 195–229. New York: Wiley
7. Schweiger A. 1991. *Angew. Chem. Int. Ed. Engl.* 30:265–92
8. Jeschke G, Schweiger A. 1995. *J. Magn. Reson. A* 119:45–52
9. Jeschke G, Schweiger A. 1997. *J. Chem. Phys.* 106:9979–91
10. Dinse KP, Biehl R, Möbius K. 1974. *J. Chem. Phys.* 61:4335–41
11. Angerhofer A, Bittl R. 1996. *Photochem. Photobiol.* 63:11–38
12. Lubitz W, Feher G. 1999. *Appl. Magn. Reson.* 17:1–48
13. Teutloff C, MacMillan F, Bittl R, Lendzian F, Lubitz W. 1998. See Ref. 246, pp. 607–10
14. Rohrer M, MacMillan F, Prisner TF, Gardiner AT, Möbius K, Lubitz W. 1998. *J. Phys. Chem. B* 102:4648–57
15. Gilchrist ML, Ball JA, Randall DW, Britt RD. 1995. *Proc. Natl. Acad. Sci. USA* 92:9545–49
16. Force DA, Randall DW, Britt RD, Tang XS, Diner BA. 1995. *J. Am. Chem. Soc.* 117:12643–44
17. Campbell KA, Peloquin JM, Diner BA, Tang XS, Chisholm DA, Britt RD. 1997. *J. Am. Chem. Soc.* 119:4787–88
18. Mino H, Kawamori A, Ono TA. 2000. *Biochim. Biophys. Acta* 1457:157–65
19. DiValentin M, Kay CWM, Giacometti G, Möbius K. 1996. *Chem. Phys. Lett.* 824:434–41
20. Lendzian F, Bittl R, Lubitz W. 1998. *Photosynth. Res.* 55:189–97
21. Bittl R, Zech SG, Teutloff C, Krabben L, Lubitz W. 1998. See Ref. 246, pp. 509–14
22. Faller P, Maly T, Rutherford AW, MacMillan F. 2001. *Biochemistry.* 39 40:320–26
23. Veselov AV, Osborne JP, Gennis RB, Scholes CP. 2000. *Biochemistry* 39:3169–75
24. Warncke K, McCracken J. 1995. *J. Chem. Phys.* 103:6839–40
25. Medina M, Cammack R. 1996. *J. Chem. Soc. Perkin Trans.* 2:633–38
26. Medina M, Lostao A, Sancho J, Gomez–Moreno C, Cammack R, et al. 1999. *Biophys. J.* 77:1712–20
27. Hoffman BM, Roberts JE, Brown TG, Kang CH, Margoliash E. 1979. *Proc. Natl. Acad. Sci. USA* 76:6132–36
28. Sivaraja M, Goodin DB, Smith M, Hoffman BM. 1989. *Science* 245:738–40
29. van Dam PJ, Willems JP, Schmidt PP, Pötsch S, Barra AL, et al. 1998. *J. Am. Chem. Soc.* 120:5080–85
30. Bennati M, Farrar CT, Bryant JA, Inati SJ, Weis V, et al. 1999. *J. Magn. Reson.* 138:232–43
31. Thomann H, Mims WB. 1992. *Pulsed Magnetic Resonance: NMR, ESR, Optical*, ed. DMS Bagguley, DM Slingsby, pp. 362–89. London/New York: Oxford Univ. Press
32. Kroneck PMH, Kastrau DHW, Schumacher W, Hole UH, Neese F, Zumft WG. 1997. In *Bioinorganic Chemistry*, ed. AX Trautwein, pp. 710–24. New York: Wiley—VCH Verlag GmbH
33. Huttermann J. 1997. In *Bioinorganic Chemistry*, ed. AX Trautwein, pp. 696–709. New York: Wiley—VCH Verlag GmbH
34. Cammack R, Gay E, Shergill JK. 1999. *Coord. Chem. Rev.* 190–192:1003–22
35. Lee HI, Doan PE, Hoffman BM. 1999. *J. Magn. Reson.* 140:91–107

36. Gurbiel RJ, Peoples R, Doan PE, Cline JF, McCracken J, et al. 1993. *Inorg. Chem.* 32:1813–19
37. Hansen AP, Britt RD, Klein MP, Bender CJ, Babcock GT. 1993. *Biochemistry* 32:13718–24
38. Fan C, Doan PE, Davoust CE, Hoffman BM. 1992. *J. Magn. Reson.* 98:62–72
39. Gromov I, Krymov V, Manikandan P, Arieli D, Goldfarb D. 1999. *J. Magn. Reson.* 139:8–17
40. Tan X, Poyner R, Reed GH, Scholes CP. 1993. *Biochemistry* 32:7799–810
41. Tan X, Bernardo M, Thomann H, Scholes CP. 1993. *J. Chem. Phys.* 98:5147–57
42. Peloquin JM, Campbell KA, Britt RD. 1998. *J. Am. Chem. Soc.* 120:6840–41
43. Manikandan P, Carmieli R, Shane T, Kalb AJ, Goldfarb D. 2000. *J. Am. Chem. Soc.* 122:3488–94
44. Doi K, McCracken J, Peisach J, Aisen P. 1988. *J. Biol. Chem.* 263:5757–63
45. Thomann H, Bernardo M, McCormick JM, Pulver S, Andersson KK, et al. 1993. *J. Am. Chem. Soc.* 115:8881–82
46. Hoffman BM. 1994. *J. Phys. Chem.* 98:11657–65
47. DeRose VJ, Woo JCG, Hawe WP, Hoffman BM, Silverman RB. 1996. *Biochemistry* 35:11085–91
48. Pollock RC, Lee HI, Cameron LM, DeRose VJ, Hales B, et al. 1995. *J. Am. Chem. Soc.* 117:8686–87
49. Thomann H, Bernardo M, Adams MWW. 1991. *J. Am. Chem. Soc* 13:7044–46
50. Fan C, Kennedy MC, Beinert H, Hoffman BM. 1992. *J. Am. Chem. Soc.* 114:374–75
51. Doan PE, Fan C, Hoffman BM. 1994. *J. Am. Chem. Soc.* 116:1033–41
52. Shergill JK, Butler CS, White AC, Cammack R, Mason JR. 1994. *Biochem. Soc. Trans.* 22:288S
53. Thomann H, Bernardo M, Goldfarb D, Kroneck PMH, Ullrich V. 1995. *J. Am. Chem. Soc.* 117:8243–51
54. Goldfarb D, Bernardo M, Thomann H, Kroneck PMH, Ullrich V. 1996. *J. Am. Chem. Soc.* 118:2686–93
55. Lee HI, Dexter AF, Fann YCh, Lakner FJ, Hager LP, Hoffman BM. 1997. *J. Am. Chem. Soc.* 119:4059–69
56. Mims WB, Nassau K, McGee JD. 1961. *Phys. Rev.* 123:2059
57. Cowen JA, Kaplan DE. 1961. *Phys. Rev.* 124:1098–101
58. Mims WB. 1972. *Phys. Rev. B* 5:2409–19
59. Shubin AA, Dikanov SA. 1983. *J. Magn. Reson.* 52:1
60. Ponti A. 1997. *J. Magn. Reson.* 127:87–104
61. Dikanov SA, Tsvetkov YD. 1992. In *Electron Spin Echo Envelope Modulation (ESEEM) Spectroscopy*, ed. SA Dikanov, YD Tsvetkov, pp. 334–58. Boca Raton, FL: CRC
62. Flanagan HL, Singel D. 1988. *J. Chem. Phys.* 87:25606–16
63. Höfer P, Grupp A, Mehring M. 1986. *Phys. Rev.* 33:3519–22
64. Mims WB. 1972. *Phys. Rev. B* 6:3543–45
65. Mims WB, Peisach J. 1989. In *Advanced EPR: Applications in Biology and Biochemistry*, ed. AJ Hoff, pp. 1–58. Amsterdam: Elsevier
66. Mims WB, Davis JL, Peisach J. 1990. *J. Magn. Reson.* 86:273–92
67. Zweier JJ, Peisach J, Mims WB. 1982. *J. Biol. Chem.* 257:10314–16
68. Jeschke G, Rakhmatullin R, Schweiger A. 1998. *J. Magn. Reson.* 131:261–71
69. Deligiannakis Y, Loudoudi M, Hadjiliadis N. 2000. *Coord. Chem. Rev.* 204:1–112
70. Mims WB, Peisach J. 1978. *J. Chem. Phys.* 69:4921–30
71. Deleted in proof
72. Colaneri MJ, Peisach J. 1995. *J. Am. Chem. Soc.* 117:6308–15
73. Place C, Zimmermann JL, Mulliez E, Guillot G, Bois C, Chottard JC. 1998. *Inorg. Chem.* 37:4030–39
74. McCracken J, Desai PR, Papadopoulos NJ, Villafranca JJ, Peisach J. 1988. *Biochemistry* 27:4133–37

75. Goldfarb D, Fauth JM, Farver O, Pecht I. 1992. *Appl. Magn. Reson.* 3:333–51
76. Balasubramanian S, Carr RT, Bender CJ, Peisach J, Benkovic SJ. 1993. *Adv. Exp. Med. Biol.* 338:67–70
77. Balasubramanian S, Carr RT, Bender CJ, Peisach J, Benkovic SJ. 1994. *Biochemistry* 33:8532–37
78. Crowder MW, Stewart JD, Roberts VA, Bender CJ, Tevelrakh E, et al. 1995. *J. Am. Chem. Soc.* 117:5627–34
79. Bender CJ, Casimiro DR, Peisach J, Jane-Dyson H. 1997. *J. Chem. Soc.* 93:3967–80
80. Coremans JWA, Poluektov OG, Groenen EJJ, Canters GW, Nar H, Messerschmidt A. 1997. *J. Am. Chem. Soc.* 119:4726–31
81. Kofman V, Farver O, Pecht I, Goldfarb D. 1996. *J. Am. Chem. Soc.* 118:1201–6
82. van Gastel M, Coremans JWA, Jeuken LJC, Canters GW, Groenen EJJ. 1998. *J. Phys. Chem.* 102:4462–70
83. McCracken J, Peisach J, Dooley DM. 1987. *J. Am. Chem. Soc.* 109:4064–72
84. Eaton SS, Dubach J, More KM, Eaton GR, Thurman G, Ambruso DR. 1989. *J. Biol. Chem.* 264:4776–81
85. Lu J, Bender CJ, McCracken J, Peisach J, Severns JC, McMillin DR. 1992. *Biochemistry* 31:6265–72
86. Bubacco L, Magliozzo RS, Wirt MD, Beltramini M, Salvato B, Peisach J. 1995. *Biochemistry* 34:1524–33
87. Dikanov SA, Burgard C, Hüttermann J. 1993. *Chem. Phys. Lett.* 212:493
88. Lu J, Bender CJ, McCracken J, Peisach J, Severns JC, McMillin DR. 1992. *Biochemistry* 31:6265–72
89. Utschig LM, Poluektov O, Tiede DM, Thurnauer MC. 2000. *Biochemistry* 39:2961–69
90. Hogan DA, Smith SR, Saari EA, McCracken J, Hausinger RP. 2000. *J. Biol. Chem.* 275:12400–9
91. Larsen RG, Halkides CJ, Singel DJ. 1993. *J. Chem. Phys.* 98:6704–21
92. Stoll S, Jeschke G, Willer M, Schweiger A. 1998. *J. Magn. Res.* 130:86–96
93. Hofbauer W, Bittl R. 2000. *J. Magn. Reson.* 147:226–31
94. Serpersu EH, McCracken J, Peisach J, Mildvan AS. 1988. *Biochemistry* 27:8034–44
95. LoBrutto R, Smithers GW, Reed GH, Orme-Johnson WH, Tan SL, Leigh JS Jr. 1986. *Biochemistry* 25:5654–60
96. Halkides CJ, Farrar CT, Larsen RG, Redfield AG, Singel DJ. 1994. *Biochemistry* 33:4019–35
97. Farrar CT, Halkides CJ, Singel DJ. 1997. *Structure* 5:1055–66
98. Tong L, de Vos AM, Milburn MV, Kim SH. 1991. *J. Mol. Biol.* 217:503–16
99. Buy C, Girault G, Zimmermann JL. 1996. *Biochemistry* 35:9880–91
100. Girault G, Berger G, Zimmermann JL. 1998. *Photosynth. Res.* 57:253–66
101. Houseman ALP, Morgan L, LoBrutto R, Frasch WD. 1994. *Biochemistry* 33: 4910–17
102. Houseman ALP, LoBrutto R, Frasch WD. 1995. *Biochemistry* 34:3277–85
103. Espe MP, Hosler JP, Ferguson-Miller S, Babcock GT, McCracken J. 1995. *Biochemistry* 34:7593–602
104. Morrissey SR, Horton TE, Grant CV, Hoogstraten CG, Britt RD, DeRose VJ. 1999. *J. Am. Chem. Soc.* 121:9215–18
105. Lorigan GA, Britt RD, Kim JH, Hille R. 1994. *Biochim. Biophys. Acta* 1185:284–94
106. Kurshev VV, Kevan L, Basu P, Enemark J. 1995. *J. Phys. Chem.* 99:11288–91
107. Pacheco A, Basu P, Borbat P, Raitsimring AM, Enemark JH. 1996. *Inorg. Chem.* 35:7001–8
108. Raitsimring AM, Pacheco A, Enemark JH. 1998. *J. Am. Chem. Soc.* 120:11263–78
109. Astashkin AV, Mader ML, Pacheco A, Enemark JH, Raitsimring AM. 2000. *J. Am. Chem. Soc.* 122:5294–302
110. De Groot A, Hoff AJ, De Beer R, Scheer H. 1985. *Chem. Phys. Lett.* 113:286–90

111. Käß H, Lubitz W. 1996. *Chem. Phys. Lett.* 251:193–203
112. Mac M, Bowlby NR, Babcock GT, McCracken J. 1998. *J. Am. Chem. Soc.* 120:13215–23
113. Hanley J, Deligiannakis Y, MacMillan F, Bottin H, Rutherford AW. 1997. *Biochemistry* 36:11543–49
114. Bosch MK, Gast P, Hoff AJ, Spoyalov AP, Tsvetkov YuD. 1995. *Chem. Phys. Lett.* 239:306–12
115. Lendzian F, Rautter J, Kaess H, Gardiner A, Lubitz W. 1996. *Ber. Bunsen-Ges.* 100:2036–40
116. Gardiner AT, Zech SG, MacMillan F, Kaess H, Bittl R, et al. 1999. *Biochemistry* 38:11773–87
117. Deligiannakis Y, Hanley J, Rutherford AW. 2000. *J. Am. Chem. Soc.* 121:7653–64
118. Grimaldi S, MacMillan F, Ostermann T, Michel H, Ludwig B, Prisner T. 2001. *Biochemistry* 40:1037–43
119. Warncke K, McCracken J, Babcock GT. 1994. *J. Am. Chem. Soc.* 116:7332–40
120. Tang XS, Randall DW, Force DA, Diner BA, Britt RD. 1996. *J. Am. Chem. Soc.* 118:7638–39
121. Britt RD, Zimmermann JL, Sauer K, Klein MP. 1989. *J. Am. Chem. Soc.* 111:3522–32
122. DeRose VJ, Yachandra VK, McDermott AE, Britt RD, Sauer K, Klein MP. 1991. *Biochemistry.* 30:1335–41
123. Tang XS, Diner BA, Larsen BS, Gilchrist ML, Lorigan GA, Britt RD. 1994. *Proc. Natl. Acad. Sci. USA* 91:704–8
124. Ivancich A, Barynin VV, Zimmermann JL. 1995. *Biochemistry* 34:6628–39
125. Dorlet P, Valentin MD, Babcock GT, McCracken JL. 1998. *J. Phys. Chem. B* 102:8239–47
126. Britt RD, Peloquin JM, Campbell KA. 2000. *Annu. Rev. Biophys. Biomol. Struct.* 29:463–95
127. Deligiannakis Y, Hanley J, Rutherford AW. 2000. *J. Am. Chem. Soc.* 122:400–1
128. Martinez JI, Alonso PJ, Gomez-Moreno C, Medina M. 1997. *Biochemistry* 36:15526–37
129. Warncke K, Brooks HB, Babcock GT, Davidson VL, McCracken J. 1993. *J. Am. Chem. Soc.* 115:6464–65
130. Warncke K, Brooks HB, Lee HI, McCracken J, Davidson VL, Babcock GT. 1995. *J. Am. Chem. Soc.* 117:10063–75
131. Ke SC, Warncke K. 1999. *J. Am. Chem. Soc.* 121:9922–27
132. Milov AD, Ponomarev AB, Tsvetkov YuD. 1984. *Chem. Phys. Lett.* 110:67–72
133. Larsen RG, Singel DJ. 1993. *J. Chem. Phys.* 98:5134–46
134. Martin RE, Pannier M, Diederich F, Gramlich V, Hubrich M, Spiess HW. 1998. *Angew. Chem. Int. Ed.* 37:2834–37
135. Pannier M, Veit S, Godt A, Jeschke G, Spiess HW. 2000. *J. Magn. Res.* 142:331–40
136. Rangan SK, Bhagat VR, Sastry VSS, Venkataraman B. 1979. *J. Magn. Res.* 33:227–40
137. Maresch GG, Weber M, Dubinskii AA, Spiess HW. 1992. *Chem. Phys. Lett.* 193:134–40
138. Kurshev VV, Raitsimring AM, Tsvetkov YuD. 1989. *J. Magn. Reson.* 81:441–54
139. Raitsimring A, Peisach J, Lee HC, Chen X. 1992. *J. Phys. Chem.* 96:3526–31
140. Raitsimring A, Crepeau RH, Freed JH. 1995. *J. Chem. Phys.* 102:8746–62
141. Saxena S, Freed JH. 1996. *Chem. Phys. Lett.* 251:102–10
142. Borbat PP, Freed JH. 1999. *Chem. Phys. Lett.* 313:145–54
143. Berliner LJ. 2000. *Biological Magnetic Resonance: Distance Measurements in Biological Systems by EPR*, ed. GR Eaton, SS Eaton, LJ Berliner. New York: Kluwer Academic
144. Astashkin AV, Kodera Y, Kawamori A. 1994. *Biochim. Biophys. Acta* 1187:89–93

145. Shigemori K, Hara H, Kawamori A, Akabori K. 1998. *Biochim. Biophys. Acta* 1363:187–98
146. Astashkin AV, Hara H, Kawamori A. 1998. *J. Chem. Phys.* 108:3805–12
147. Persson M, Harbridge JR, Hammarström P, Mitri R, Mårtensson LG, et al. *Biophys. J.* Submitted
148. Kulikov AV, Likhtenstein GI. 1977. *Adv. Mol. Relax. Interact. Process* 10:47
149. Evelo RG, Styring S, Rutherford AW, Hoff AJ. 1989. *Biochim. Biophys. Acta* 973:428–42
150. Hirsh DJ, Beck WF, Innes JB, Brudvig GW. 1992. *Biochemistry* 31:532–41
151. Kodera Y, Takura K, Kawamori A. 1992. *Biochim. Biophys. Acta* 1101:23–32
152. Koulougliotis D, Innes JB, Brudvig GW. 1994. *Biochemistry* 33:11814–22
153. Koulougliotis D, Tang XS, Diner BA, Brudvig GW. 1995. *Biochemistry* 34:2850–56
154. Deligiannakis Y, Rutherford AW. 1996. *Biochemistry* 35:11239–46
155. Hirsh DJ, Beck WF, Lynch JB, Que L, Brudvig GW. 1992. *J. Am. Chem. Soc.* 114:7475–81
156. Dzuba SA, Kodera Y, Hara H, Kawamori A. 1993. *J. Magn. Reson. A* 102:257–60
157. Kodera Y, Dzuba SA, Hara H, Kawamori A. 1994. *Biochim. Biophys. Acta* 1186:91–99
158. Hara H, Kawamori A. 1997. *Appl. Magn. Reson.* 13:241–57
159. Budker V, Du JL, Seiter M, Eaton GR, Eaton SS. 1995. *Biophys. J.* 68:2531–42
160. Zhou Y, Bowler BE, Lynch K, Eaton SS, Eaton GR. 2000. *Biophys. J.* 79:1039–52
161. Hyde JS, Dalton LR. 1972. *Chem. Phys. Lett.* 16:568–72
162. Freed JH. 1979. In *Time Domain Electron Spin Resonance*, ed. L Kevan, RN Schwartz, pp. 31–66. New York: Wiley
163. Millhauser GL, Freed JH. 1984. *J. Chem. Phys.* 81:37–48
164. Marsh D. 1980. *Biochemistry* 19:1632–37
165. Beth AH, Robinson BH. 1989. In *Biological Magnetic Resonance: Spin Labeling: Theory and Applications*, ed. LJ Berliner, J Reubens, 8:179–253. New York: Plenum
166. Kar L, Millhauser GL, Freed JH. 1984. *J. Phys. Chem.* 88:3951–56
167. Dzuba SA, Watari H, Shimoyama Y, Maryasov AG, Kodera Y, Kawamori A. 1995. *J. Magn. Reson. A* 115:80
168. Lee S, Budil DE, Freed JH. 1994. *J. Chem. Phys.* 101:5529–58
169. Saffman PG, Delbrück M. 1975. *Proc. Natl. Acad. Sci. USA* 72:3111–13
170. Freed JH. 1964. *J. Chem. Phys.* 41:2077–83
171. Ge M, Field KA, Aneja R, Holowka D, Baird B, Freed JH. 1999. *Biophys. J.* 77:925–33
172. Liang Z, Freed JH, Keyes RS, Bobst AM. 2000. *J. Phys. Chem. B* 104:5372–81
173. Kar L, Johnson ME, Bowman MK. 1987. *J. Magn. Reson.* 75:397–413
174. Buitink J, Dzuba SA, Hoekstra FA, Tsvetkov YD. 2000. *J. Magn. Reson.* 142:364–68
175. Pinheiro TJT, Bratt PJ, Davis IH, Doetschman DC, Watts A. 1993. *J. Chem. Soc. Perkin Trans.* 211:2113–17
176. van der Struijf C, Pelupessy TPH, van Faassen EE, Levine YK. 1996. *J. Magn. Reson. B* 111:158–67
177. Yin JJ, Feix JB, Hyde JS. 1990. *Biophys. J.* 58:713–20
178. Altenbach C, Froncisz W, Hyde JS, Hubbell WL. 1989. *Biophys. J.* 56:1183–91
179. Steinhoff HJ, Savitsky A, Wegener C, Pfeiffer M, Plato M, Möbius K. 2000. *Biochim. Biophys. Acta* 1457:253–62
180. Prisner TF. 1997. In *Advances in Magnetic and Optical Resonance*, ed. WS Warren, 20:245–300. San Diego: Academic
181. Rohrer M, Gast P, Möbius K, Prisner TF. 1996. *Chem. Phys. Lett.* 259:523–30
182. Bittl R, Zech SG. 1997. *J. Phys. Chem. B* 101:1429–36

183. Stehlik D, Möbius K. 1997. *Annu. Rev. Phys. Chem.* 48:739–78
184. Kim SS, Weisman SI. 1976. *J. Magn. Reson.* 24:167–69
185. Hoff AJ, Gast P, Romijn JC. 1977. *FEBS Lett.* 73:185–90
186. Stehlik D, Bock CH, Thurnauer MC. 1989. In *Advanced EPR: Applications in Biology and Biochemistry*, ed. AJ Hoff, pp. 371–404. Amsterdam: Elsevier
187. Snyder SW. 1993. In *The Photosynthetic Reaction Center*, ed. J Deisenhofer, J Norris, 2:285–330. New York: Academic
188. Prisner TF, van der Est A, Bittl R, Lubitz W, Stehlik D, Möbius K. 1995. *Chem. Phys.* 194:361–79
189. Van der Est A, Prisner TF, Bittl R, Fromme P, Lubitz W, Möbius K, Stehlik D. 1997. *J. Phys. Chem. B* 101:1437–43
190. Salikhov KM, Bock CH, Stehlik D. 1990. *Appl. Magn. Res.* 1:195–211
191. Kothe G, Weber S, Bittl R, Ohmes E, Thuranuer MC, Norris JR. 1991. *Chem. Phys. Lett.* 186:474–80
192. Weber S, Ohmes E, Thurnauer MC, Norris JR, Kothe G. 1996. In *Reaction Centres of Photosynthetic Bacteria: Structure and Dynamics*, ed. ME Michel-Beyerle, pp. 341–51. Berlin: Springer
193. Thurnauer MC, Clark C. 1984. *Photochem. Photobiol.* 40:381–86
194. Salikhov KM, Kandrashkin YE, Salikhov AK. 1992. *Appl. Magn. Reson.* 3:199–216
195. Zwanenburg G, Hore PJ. 1995. *J. Magn. Reson.* 114:139–46
196. Jeschke G, Bittl R. 1998. *Chem. Phys. Lett.* 294:323–31
197. Dzuba SA, Gast P, Hoff AJ. 1995. *Chem. Phys. Lett.* 236:595–602
198. Zech SG, Lubitz W, Bittl R. 1996. *Ber. Bunsen-Ges.* 100:2041–44
199. Dzuba SA, Hoff AJ. 1997. *Chem. Phys. Lett.* 268:273–79
200. Hara H, Dzuba SA, Kawamori A, Akabori K, Tomo T, et al. 1997. *Biochim. Biophys. Acta* 1322:77–85
201. Zech SG, Kurreck J, Eckert HJ, Renger G, Lubitz W, Bittl R. 1997. *FEBS Lett.* 414:454–56
202. Bittl R, Zech SG, Fromme P, Witt HT, Lubitz W. 1997. *Biochemistry* 36:12001–4
203. Zech SG, Kurreck J, Renger G, Lubitz W, Bittl R. 1999. *FEBS Lett.* 442:79–82
204. Yoshii T, Hara H, Kawamori A, Akabori K, Iwaki M, Itoh S. 1999. *Appl. Magn. Reson.* 16:565–80
205. Yoshii T, Kawamori A, Tonaka M, Akabori K. 1999. *Biochim. Biophys. Acta* 1413:43–49
206. Borovykh IV, Dzuba SA, Proskuryakov II, Gast P, Hoff AJ. 1998. *Biochim. Biophys. Acta* 1363:182–86
207. Zech SG, Bittl R, Gardiner AT, Lubitz W. 1997. *Appl. Magn. Reson.* 13:517–29
208. Tang J, Norris JR. 1995. *Chem. Phys. Lett.* 233:192–200
209. Dzuba SA, Bosch MK, Hoff AJ. 1996. *Chem. Phys. Lett.* 248:427–33
210. Dei A, Gatteschi D, Pardi LA, Barra AL, Brunel LC. 1990. *Chem. Phys. Lett.* 175:589–91
211. Burghaus O, Plato M, Rohrer M, Möbius K, MacMillan F, Lubitz W. 1993. *J. Phys. Chem.* 97:7639–47
212. Prisner TF, McDermott AE, Un S, Norris JR, Thurnauer MC, Griffin RG. 1993. *Proc. Natl. Acad. Sci. USA* 90:9485–88
213. Gerfen GJ, Bellew BF, Un S, Bollinger JM, Stubbe JA, et al. 1993. *J. Am. Chem. Soc.* 115:6420–21
214. Möbius K. 1993. In *Biological Magnetic Resonance: EMR of Paramagnetic Molecules*, ed. LJ Berliner, J Reubens, 13:253–74. New York: Plenum
215. Bratt PJ, Rohrer M, Krzystek J, Evans MCW, Brunel LC, Angerhofer A. 1997. *J. Phys. Chem. B* 101:9686–89
216. Möbius K. 2000. *Chem. Soc. Rev.* 29:129–39
217. Dorlet P, Rutherford AW, Un S. 2000. *Biochemistry* 39:7826–34
218. Bresgunov AY, Dubinskii AA, Krimov VN, Petrov YG, Poluektov OG, Lebedev YS. 1991. *Appl. Magn. Reson.* 2:715–28

219. Burghaus O, Rohrer M, Götzinger T, Plato M, Möbius K. 1992. *Meas. Sci. Technol.* 3:765–74
220. Disselhorst JAJM, van der Meer H, Poluektov OG, Schmidt J. 1995. *J. Magn. Reson. A* 115:183–88
221. Becerra LR, Gerfen GJ, Bellew BF, Bryant JA, Hall DA, et al. 1995. *J. Magn. Reson. A* 117:28–40
222. Earle KA, Tipikin DS, Freed JH. 1996. *Rev. Sci. Instrum.* 67:2502–13
223. Smith GM, Lesurf JCG, Mitchell RH, Riedi PC. 1998. *Rev. Sci. Instrum.* 69:3924–37
224. Fuchs M, Prisner T, Möbius K. 1999. *Rev. Sci. Instrum.* 70:3681–83
225. Grinberg OY, Dubinskii AA, Shuvalov VF, Oranskii LG, Kurochkin VI, Lebedev YS. 1976. *Dokl. Phys. Chem.* 230:923–30 (In English)
226. Weber RT, Disselhorst JAJM, Prevo LJ, Schmidt J, Wenckebach WT. 1988. *J. Magn. Reson.* 81:129–44
227. Prisner TF, Un S, Griffin RG. 1992. *Isr. J. Chem.* 32:357–63
228. Prisner TF, Rohrer M, Möbius K. 1994. *Appl. Magn. Reson.* 7:167–83
229. Kutter C, Moll HP, van Tol J, Zuckermann H, Maan JC, Wyder P. 1995. *Phys. Rev. Lett.* 74:2925–28
230. Moll HP, Kutter C, van Tol J, Zuckermann H, Wyder P. 1999. *J. Magn. Reson.* 137:46–58
231. Bellew BF, Halkides CJ, Gerfen GJ, Griffin RG, Singel D. 1996. *Biochemistry* 35:12186–93
232. Geyer M, Schweins T, Herrmann C, Prisner T, Wittinghofer A, Kalbitzer HR. 1996. *Biochemistry* 35:10308–20
233. Rohrer M, Prisner TF, Brügmann O, Käß H, Spörner M, et al. 2001. *Biochemistry* In press
234. Käß H, MacMillan F, Ludwig B, Prisner TF. 2000. *J. Phys. Chem. B* 104:5362–71
235. Müller F, Hopkins MA, Coron N, Grynberg M, Brunel LC, Martinez G. 1989. *Rev. Sci. Instrum.* 60:3681–84
236. Hassan AK, Pardi LA, Krzystek J, Sienkiewicz A, Goy P, et al. 2000. *J. Magn. Reson.* 142:300–12
237. Rohrer M, Plato M, MacMillan F, Grishin Y, Lubitz W, Möbius K. 1995. *J. Magn. Reson. A* 116:59–66
238. Coremans JWA, Poluektov OG, Groenen EJJ, Canters GW, Nar H, Messerschmidt A. 1996. *J. Am. Chem. Soc.* 118:12141–53
239. Goldfarb D, Strohmaier KG, Vaughan DEW, Thomann H, Poluektov OG, Schmidt J. 1996. *J. Am. Chem. Soc.* 118:4665–71
240. Mehring M, Höfer P, Grupp A. 1987. *Ber. Bunsenges. Phys. Chem.* 91:1132–37
241. Epel B, Goldfarb D. 2000. *J. Magn. Reson.* 146:196–203
242. Bloeß A, Möbius K, Prisner TF. 1998. *J. Magn. Reson.* 134:30–35
243. Coremans JWA, van Gastel M, Poluektov OG, Groenen EJJ, den Blaauwen T, et al. 1995. *Chem. Phys. Lett.* 235:202–10
244. Gerfen GJ, Bellew BF, Griffin RG, Singel DJ, Ekberg CA, Whittaker JW. 1996. *J. Phys. Chem.* 100:16739–48
245. Rohrer M, Brügmann O, Kinzer B, Prisner TF. In preparation
246. Garab G. 1998. *Photosynthesis: Mechanisms and Effect*, Vol. 1. Dordrecht, The Netherlands: Kluwer Academic
247. Peisach J. 1995. *Proc. Int. Conf. Bioradicals Detected ESR Spectroscopy*, ed. H Ohya-Nishiguchi, L Packer, pp. 203–15 Basel: Birkhauser

Annual Review of Physical Chemistry
Volume 52, 2001

CONTENTS

A Free Radical, *Alan Carrington* 1
State-to-State Chemical Reaction Dynamics in Polyatomic Systems: Case Studies, *James J Valentini* 15
Recent Progress in Infrared Absorption Techniques for Elementary Gas-Phase Reaction Kinetics, *Craig A Taatjes, John F Hershberger* 41
Surface Biology of DNA by Atomic Force Microscopy, *Helen G Hansma* 71
On the Characteristics of Migration of Oligomeric DNA in Polyacrylamide Gels and in Free Solution, *Udayan Mohanty, Larry McLaughlin* 93
Mechanisms and Kinetics of Self-Assembled Monolayer Formation, *Daniel K Schwartz* 107
Crossed-Beam Studies of Neutral Reactions: State-Specific Differential Cross Sections, *Kopin Liu* 139
Coincidence Spectroscopy, *Robert E Continetti* 165
Spectroscopy and Hot Electron Relaxation Dynamics in Semiconductor Quantum Wells and Quantum Dots, *Arthur J Nozik* 193
Ratiometric Single-Molecule Studies of Freely Diffusing Biomolecules, *Ashok A Deniz, Ted A Laurence, Maxime Dahan, Daniel S Chemla, Peter G Schultz, Shimon Weiss* 233
Time-Resolved Photoelectron Spectroscopy of Molecules and Clusters, *Daniel M Neumark* 255
Pulsed EPR Spectroscopy: Biological Applications, *Thomas Prisner, Martin Rohrer, Fraser MacMillan* 279
Fast Protein Dynamics Probed with Infrared Vibrational Echo Experiments, *Michael D Fayer* 315
Structure and Bonding of Molecules at Aqueous Surfaces, *GL Richmond* 357
Light Emitting Electrochemical Processes, *Neal R Armstrong, R Mark Wightman, Erin M Gross* 391
Reactions and Thermochemistry of Small Transition Metal Cluster Ions, *PB Armentrout* 423
Spin-1/2 and Beyond: A Perspective in Solid State NMR Spectroscopy, *Lucio Frydman* 463
From Folding Theories to Folding Proteins: A Review and Assessment of Simulation Studies of Protein Folding and Unfolding, *Joan-Emma Shea, Charles L Brooks III* 499
Polymer Adsorption-Driven Self-Assembly of Nanostructures, *Arup K Chakraborty, Aaron J Golumbfskie* 537
Biomolecular Solid State NMR: Advances in Structural Methodology and Applications to Peptide and Protein Fibrils, *Robert Tycko* 575
Photofragment Translational Spectroscopy of Weakly Bound Complexes: Probing the Interfragment Correlated Final State Distributions, *L Oudejans, RE Miller* 607
Coherent Nonlinear Spectroscopy: From Femtosecond Dynamics to Control, *Marcos Dantus* 639
Electron Transmission through Molecules and Molecular Interfaces, *Abraham Nitzan* 681

Early Events in RNA Folding, *D Thirumalai, Namkyung Lee, Sarah A Woodson, DK Klimov* 751

Laser-Induced Population Transfer by Adiabatic Passage Techniques, *Nikolay V Vitanov, Thomas Halfmann, Bruce W Shore, Klaas Bergmann* 763

The Dynamics of "Stretched Molecules": Experimental Studies of Highly Vibrationally Excited Molecules with Stimulated Emission Pumping, *Michelle Silva, Rienk Jongma, Robert W Field, Alec M Wodtke* 811